Soliton-like excitations in a deformable spin model

2004 J. Phys.: Condens. Matter 16 373

(http://iopscience.iop.org/0953-8984/16/3/016)

INSTITUTE OF PHYSICS PUBLISHING JOURNAL OF PHYSICS: CONDENSED MATTER

J. Phys.: Condens. Matter **16** (2004) 373–403 PII: S0953-8984(04)67006-8

Soliton-like excitations in a deformable spin model

Jean-Pierre Nguenang[1,2,3,4], **Aurelien J Kenfack**[2] **and Timoleon C Kofané**[2]

[1] The Abdus Salam International Centre for Theoretical Physics, PO Box 506, Strada Costiera, II-34014 Trieste, Italy
[2] Laboratoire de Mécanique, Faculté des Sciences Université de Yaoundé I, BP 812, Yaoundé, Cameroun
[3] Laboratoire de Physique, Ecole Normale Supérieure de Lyon, 46 Allée d'Italie, 69364 Lyon Cedex 07, France

E-mail: nguenang@yahoo.com

Received 4 August 2003
Published 9 January 2004
Online at stacks.iop.org/JPhysCM/16/373 (DOI: 10.1088/0953-8984/16/3/016)

Abstract

Nonlinear excitations in a one-dimensional deformable, discrete, classical, ferromagnetic chain are numerically investigated. In the continuum limit the equations of motion are reduced to a Klein–Gordon equation, with a Remoissenet–Peyrard substrate potential. From a numerical computation of the discrete system with a suitable choice of the deformability parameters, the soliton solutions are shown to exist and move both with a monotonic oscillating (i.e. nanopteron) and a monotonic nonoscillating tail, and also with a non-oscillating tail but with a splitting propagating shape. The stability of all these various soliton shapes is confirmed numerically in a range of the reduced magnetic fields greater than for a rigid magnetic chain i.e. $0 \leqslant b \leqslant 0.33$. From a kink–antikink and a kink–kink colliding simulation, we found various effects, including a bound state of a kink and an antikink, as well as a moving kink profile with higher topological charge that appears to be the bound state of two kinks. For some values of the deformability parameter, with a suitable choice of the initial velocity, we observed that the presence of an internal mode leads to the combination of an attractive and a repulsive phenomenon, that arises when the kink–kink collision is engaged. The fact that this collision happens only in the centre of the magnetic chain with the presence of a minimal distance between the two kinks as long as the collision is produced is also a feature of the deformability effect in the dynamics of a magnetic chain. From our results, it appears that the value of the shape parameter of the substrate potential or the modified Zeeman energy is a factor of utmost importance when modelling magnetic chains.

(Some figures in this article are in colour only in the electronic version)

[4] Permanent address: Condensed Matter Laboratory, Department of Physics, Faculty of Science, University of Douala, PO Box: 24157, Douala, Cameroon.

1. Introduction

It is commonly well acknowledged that the investigation of nonlinear waves and soliton-like excitations has provided fruitful and interesting outcomes in many areas of condensed matter physics [1]: dislocation in crystals [2–4], planar domain walls in ferromagnets [5] and ferroelectrics [6–8], nonlinear spin waves [9, 10], charge carriers in weakly pinned charge-density wave condensates [11], incommensurate systems [12, 13] and bond-alternation domain walls in poly-acetylene [14], to cite just a few examples. Two-dimensional (2D) systems, as well as one-dimensional (1D) models, have attracted great attention.

In the context of 2D models that are applied to magnetic films and superlattices, the interest has been driven by enormous experimental advances in the growth and characterization techniques of these materials, as well as investigations which have led to the realization of high quality samples and the discovery of many new and interesting phenomena, such as the oscillatory exchange coupling between ferromagnetic films that are separated by non-magnetic spacers [15] and the giant magneto-resistance effect [16]. Owing to these advances, the determination of the ground state of the magnetic model through a uniaxial antiferromagnet in the presence of an applied magnetic field was formulated as a 2D area-preserving map; the results were consistent with the experimental data on Fe/Cr(211) superlattices [17] and other theoretical works [18, 19]. The advances made in the characterization of these magnetic materials help in setting up good tools for magnetic bubble propagation through solitary configurations with particle-like properties. These solitary magnetic bubbles have played, in recent years, a vital role in the rapid advancement of information technology. In the specific context of the 1D model, nonlinear excitations in a quasi-one-dimensional magnetic system have received much theoretical, experimental and computational attention in recent years [9, 20–24].

In most of the aforementioned studies related to the dynamics of magnetic chains, the part of the symmetry-breaking potential introduced into the system through the Zeeman energy contribution under the action of an external magnetic field leads to the sine–Gordon picture when the continuum approximation is used and the anisotropy is assumed to be extremely strong. The important question of relaxing the simplified assumptions mentioned above has been much investigated, mostly by treating these assumptions as if they were independent from each other. The investigation of the ferromagnetic chain with finite anisotropy in the classical continuum limit [25–28] revealed the existence of out-of-plane instabilities, as well as a soliton spectrum quite different from the sine–Gordon results. Similar studies of the quantum sine–Gordon equation [29], as well as a discrete sine–Gordon chain [30, 31], have contributed to our understanding of the modelization of a 1D solid.

However, in real magnetic systems, whenever the above-mentioned assumptions are used in order to approach the macroscopic description of their dynamics, it remains a fact that, for a more accurate investigation, the possibility that the potential can deviate strongly from the sinusoidal one should be taken into account. This behaviour can be induced in the system by the generation of the nonlinear harmonics in the sinusoidal potential that are due to microscopic structures and the influence of various interactions. The magneto-elastic interactions can arise, for instance, either from the strain derivatives of the crystalline electric field, as a one-ion effect, eventually leading to a two-ion interaction, or from a distance-dependent-exchange interaction or otherwise from a local moment formation or change. Such a microscopic situation may lead to isotropic, as well as anisotropic, macroscopic deformations. Among the different effects, it is often normal to distinguish precisely the magneto-volume effect, which is a spontaneous deformation at a magnetic ordering, the positive and negative Joule magnetostriction, which is the field-induced parallel and perpendicular deformation of the

material, and thermal expansion or contraction of magnetic origin. All these various effects lead to new shapes of the domain wall that are consequences of the appearance of new harmonics on the substrate potential [32, 33].

In such a context as underscored above, recently, one of us [34] began by putting forward a novel model in which the Hamiltonian was characterized by the nearest neighbour exchange energy, the single-ion anisotropy and a deformable Zeeman energy. In that paper, the attention was focused on the situation where the Zeeman energy can be varied continuously as a function of the deformability parameter r. While taking the continuum limit, he showed that such a magnetic system could be mapped approximately onto the one-dimensional deformable sG equation at extremely low temperatures, from which implicit soliton solutions that depend on the parameter r could be derived. In spite of the novelty of that model, it was somewhat limited in its applicability to a wide range of real magnetic systems. Pursuing then the same idea with a spirit of generalization, we have very recently introduced a 1D spin model with a modified Zeeman energy that led to the nonlinear deformable periodic substrate potential. We have shown that the range of the deformability parameter and, consequently, the shape of the substrate potential is a factor of utmost importance when modelling a magnetic physical system [35]. Henceforth, the range of the magnetic field for the stability of the nonlinear excitations propagating in the system is enhanced. The static critical magnetic field disappears for the shape potential parameters $r \neq 0$. Moreover, the model shows very different phenomenologies that comprise a ballistic, a diffusive and a stochastic behaviour. Therefore, the deformability provides insight into unusual behaviours that may be typical of multivariate dynamical magnetic systems. Hence, important and interesting new features are then introduced in the dynamics of ferromagnetic chains through the propagation and the collision processes of the findings.

Our aims in this paper are firstly to show that limits found for sG magnetic solitons can be extended if one considers a generalized model, confirming therefore our result obtained in [35], secondly to show that properties determined for one-component deformable soliton model are still valid for a magnetic system where two degrees of freedom are coupled and finally to show also that carrying out a theoretical analysis through numerical simulation of the solitary waves including their interactions in a discrete ferromagnetic chain under deformability effects also leads to new features.

The material of this paper is organized as follows. In section 2, we describe the model and give its different limits and, next, we derive the discrete equations of motion. In the continuum limits, the implicit kink solutions are calculated exactly. Section 3 is devoted to the numerical studies of the soliton-like excitations in the discrete magnetic chain under deformability effects. We investigate their stability and particle-like interaction through collision processes. We consider both moving kink solutions with monotonic and oscillating tails. In section 4, we give a summary and our concluding remarks.

2. The model

In order to find a starting point that would pave the way for a classical theory for a more suitable model that can be applied to realistic one-dimensional magnetic systems, let us start by presenting some of the well known models that are used to describe magnetic spin chains.

To introduce the simplest of these models in which a relationship between magnetic domain walls and solitons, as special solutions, can be established, let us consider a magnetic chain with the Hamiltonian [5]

$$H = -J \sum_i \vec{S}_i \cdot \vec{S}_{i+1} + V(\vec{S}_i). \tag{2.1}$$

Here, the first term represents the ferromagnetic ($J > 0$) or antiferromagnetic ($J < 0$) Heisenberg exchange interaction between neighbouring spins denoted by the vectors $\vec{S}_i$ and $\vec{S}_{i+1}$. The second term is a single-spin potential that can have various forms.

If $V(\vec{S}_i) = A\sum_i (S_i^z)^2$, with J and A that are positive and negative constants, respectively, then the total Hamiltonian can describe a magnetic chain with Ising (easy-axis) symmetry. In a classical description, this Hamiltonian has two equivalent ground states $S_i^z = \pm S$. The configuration describing the transition between these equivalent ground states is the static domain wall. Its structure is determined from a competition between the exchange energy J that favours a broad wall and the anisotropy energy A that favours a narrow wall. On the other hand, we have a planar Heisenberg system if A has a negative sign ($A < 0$).

Next, we consider a model of a one-dimensional magnet with the following expression for spin potential $V(\vec{S}_i)$ [20]:

$$V(\vec{S}_i) = A\sum_i (S_i^z)^2 - g\mu_B B_x \sum_i S_i^x. \tag{2.2}$$

Thus, in the total Hamiltonian, the main effect of the magnetic field is to break the continuous symmetry. At temperature $T < (AJ)^{\frac{1}{2}}$, the single-ion anisotropy $A > 0$ enforces a small z component of spin and therefore XY-like behaviour. In addition to this condition, if the inequality $\frac{A}{JS(S+1)} \ll 4\pi^2$ is fulfilled, then quantum effects can be neglected. The spins can be treated as classical vectors

$$\vec{S}_i(z,t) = S(\cos(\theta_i)\cos(\varphi_i), \cos(\theta_i)\sin(\varphi_i), \sin(\theta_i)). \tag{2.3}$$

At zero magnetic field and for sufficiently low temperatures, the dynamic behaviour of this model is dominated by small oscillations in the difference angles $\varphi_{i+1} - \varphi_i$. The angle φ_i itself, however, can float over the entire range of $[0,\ 2\pi]$ owing to continuous symmetry in the XY plane, leading then to a damping of the corresponding oscillations of the in-plane spin components. When the applied magnetic field is non-nil, then the continuous symmetry is broken, and stable magnons, i.e. harmonic oscillations about $\varphi_i = 0$, result for increasing and highest magnetic field. However, for moderate fields, satisfying $g\mu_B BJ \leqslant T^2$, the occurrence of complete turns in φ_i remains likely. This intermediate region mostly deals with the soliton theory, based on the equivalent, which is established in the long-wavelength limits, in the system considered to a sine–Gordon (sG) system. To this end, it is necessary to relate the equations of motion for the spin degrees of freedom φ_i, θ_i to a sine–Gordon equation. In the continuum limit of long wavelength, $qa_0 \ll (2A/J)^{\frac{1}{2}}$ (where a_0 is the lattice spacing) and for magnetic fields $g\mu_B B \ll 2A$, the equations of motion read

$$\frac{\partial^2\varphi}{\partial z^2} - \frac{1}{c^2}\frac{\partial^2\varphi}{\partial t^2} = m^2\sin(\varphi) \tag{2.4a}$$

$$\theta = \frac{1}{2AS}\frac{\partial\varphi}{\partial t}. \tag{2.4b}$$

Here, $c = a_0 S(2AJ)^{1/2}$ is the characteristic velocity and $m = \{g\mu_B B/JSa_0\}^{1/2}$ plays the role of the mass. The equation of motion (2.4a) follows from the Hamiltonian density (with the energy measured in units of JS^2 and length units of the lattice spacing)

$$\mathrm{H} = \frac{1}{2}\left\{\left(\frac{\partial\varphi}{\partial z}\right)^2 + \frac{1}{c^2}\left(\frac{\partial\varphi}{\partial t}\right)^2\right\} + m^2(1-\cos(\varphi)). \tag{2.5a}$$

In the above Hamiltonian form, the last term is the so-called sine–Gordon substrate potential, i.e.

$$V(\varphi) = m^2(1-\cos(\varphi)). \tag{2.5b}$$

From Hamiltonian (2.1), another way of breaking the symmetry in the easy plane is to introduce an additional single-ion anisotropy in the x-axis. Moreover, with this new model, when a second anisotropy axis is considered, it leads to the following form for $V(\vec{S}_i)$:

$$V(\vec{S}_i) = A\sum_i (S_i^z)^2 - C\sum_i (S_i^x)^2 - g\mu_B B_x \sum_i S_i^x. \tag{2.6}$$

Here, in the resulting total Hamiltonian, J, A and C are positive constants, and the other notations are standard. This model is valid either for a 1D spin configuration of a 3D ferromagnet depending on a single coordinate z only, or for a 1D ferromagnet such as the $S = 1$ compound $[(CH_3)_3NH]NiCl_3{\cdot}2H_2O$, whose magneto-crystalline properties have been investigated in detail by Hoogerbeets *et al* [36]. In the classical limit and at low temperatures, Magyari and Thomas [37] have shown that in the limits $a = \frac{C}{A} \ll 1$ and $b = \frac{g\mu_B B_x}{2DS} \ll 1$ the equations of motion related to the rotational degree of freedom of the spins are

$$\frac{\partial^2\varphi}{\partial z^2} - \frac{\partial^2\varphi}{\partial t^2} = b\sin(\varphi) + \frac{1}{2}a\sin(2\varphi) \tag{2.7a}$$

$$\theta = \frac{\partial\varphi}{\partial t}. \tag{2.7b}$$

Equation (2.7*a*) is a double sine–Gordon (dsG) equation. It is also possible from the form

$$V(\vec{S}_i) = A\sum_i (S_i^z)^2 - g\mu_B B_y \sum_i S_i^y - g\mu_B B_x \sum_i (-1)^n S_i^x \tag{2.8}$$

of $V(\vec{S}_i)$ to modelize a 1D antiferromagnet with single-ion anisotropy in an external magnetic field, and also under a transverse or staggered magnetic field. Using then the spin parametrization introduced by Mikeska [20], the equation (2.7*a*) is the equation of motion that describes the dynamics of the in-plane angles. The corresponding Hamiltonian density (with the energy measured in units of JS^2 and length units of the lattice spacing) is given by

$$\mathrm{H} = \frac{1}{2}\left\{\left(\frac{\partial\varphi}{\partial z}\right)^2 + \frac{1}{c^2}\left(\frac{\partial\varphi}{\partial t}\right)^2\right\} + \lambda\sin^2(\varphi) + 2\nu(1-\cos(\varphi)). \tag{2.9}$$

In this Hamiltonian, the substrate potential is the dsG potential given by

$$V(\varphi) = \lambda\sin^2(\varphi) + 2\nu(1-\cos(\varphi)). \tag{2.10}$$

It can be observed that the difference between the potential given in equation (2.10) and that of equation (2.5*b*) comes from the fact that there is a second harmonic that is related to the presence of an additional equilibrium position on the substrate potential. This dsG potential then displays two harmonics with parameter λ that can be varied.

From the models of the spin chain presented above, it is possible to describe the dynamics of most of the 1D magnetic materials, but, unfortunately, for most of these materials, experimental checks of theoretical prediction are either inconsistent or not available. For instance, although a critical value of the applied magnetic field was theoretically established as $b = 1/3$ for the $CsNiF_3$ material [25, 26], it has not been proven experimentally [5]. The reason for this inconsistency comes from the fact that those theoretical models are too simple to represent real specimens, while real samples are too 'dirty' to be describing a reliable theoretical model. Very often, if a more realistic model is used, the results become too complex to have a clear physical interpretation. On the other hand, neglecting the leading effects may lead to misleading theoretical predictions. The ideal system is one in which the leading physical features are well represented by a simple theoretical model.

On varying the parameter λ of equation (2.10), it can be realized that the profile would change [35]. This situation then leads us to think about a deformable model. With this potential,

that comes from a spin chain model, we have been motivated to find a more generalized potential that would include supplementary harmonics. To this end, let us recall the Remoissenet–Peyrard potential that presents the following compact form:

$$V_{\mathrm{RP}}(\varphi, r) = (1-r)^2 \frac{1-\cos\varphi}{1+r^2+2r\cos\varphi}, \qquad |r| < 1. \tag{2.11}$$

From its profile given in [35], we notice that it displays constant amplitude with period 2π. The trivial cases $V(r = 1) = 0$ and $V(r = -1) = 2$ are ignored. This potential can be expanded in a Fourier series as

$$V(\varphi, r) = (1-r) + (1-r^2)(-\cos\varphi + r\cos 2\varphi + \cdots + (-1)r^{n-1}\cos n\varphi + \cdots). \tag{2.12}$$

Any choice of the parameter r in the range $-1 < r < 1$ enables one to change the form of the potential (i.e. to vary the weight of its harmonics) while keeping its amplitude constant and equal to two. It also happens that when $r = 0$, $V(\varphi, 0) = 1 - \cos\varphi$, i.e. the potential reduces to the familiar sG potential. One can also note that the leading term in Fourier expansion (2.12) of the potential is the sG harmonics. On the other hand, when $r \to 1$, the potential would become extremely sharp. When $r \to -1$, the inverse result is obtained, i.e. we have a potential with a flat bottom. For small values of r, the potential reduces to the dsG potential as

$$V(\varphi) \propto -\cos\varphi + r\cos 2\varphi. \tag{2.13}$$

Though the supplementary harmonics in equation (2.11) give rise to a trend quite different from that of sG or dsG models, there exist general features inherent in this process associated with the shape parameter r which enables the development of a general concept, including spin deformable models in the same spirit as the deformable model of the nonlinear Klein–Gordon system.

The model we considered in this paper is a discrete chain of classical spins with planar single-ion anisotropy. It is also subjected to deformability that is introduced into the system through a deformable Zeeman energy. We take into account exchange interactions between nearest neighbours' spins only, and we write the Hamiltonian in the following form:

$$H = -J\sum_i \vec{S}_i \cdot \vec{S}_{i+1} + A\sum_i (S_i^z)^2 + g\mu_{\mathrm{B}}(1-r)^2 B_x \cdot S \sum_i \frac{(1 - S^{-1}S_i^x)}{1 + r^2 + 2rS^{-1}S_i^x}. \tag{2.14}$$

Here, S represents the modulus of the atomic spin ($S = |\vec{S}_i|$ in units of $\hbar$), the index x on the magnetic field component indicates that the magnetic field is applied in the X axis and r is the shape parameter that varies in the range $-1 < r < 1$ as previously introduced by Remoissenet and Peyrard [38, 39]. J, A and all other notations are standard [5]. The Z direction is the direction of the chain and the easy plane is the (XY) plane. In the last term of the Hamiltonian (equation (2.14)), that corresponds to the deformable Zeeman term, the presence of $S^{-1}S_i^x = \cos(\theta_i)\cos(\varphi_i)$ in the denominator comes from the mathematical recombination of the Taylor expansion of the sinusoidal potential that is subject to the above mentioned nonlinear harmonic generation. Before proceeding, it is necessary, as we did in [35], to notice the three important limits of this Hamiltonian.

Case 1. When the deformability parameter r tends to unity, the deformable Zeeman energy becomes zero. The total Hamiltonian then reads

$$H = -J\sum_i \vec{S}_i \cdot \vec{S}_{i+1} + A\sum_i (S_i^z)^2.$$

Consequently, two situations can occur. We first have an Ising-like system if the anisotropy constant A is negative ($A < 0$), or secondly we have a planar Heisenberg system if A has a positive sign ($A > 0$). In this latter case, we notice that the magnetic compound should behave

as if it is not subjected to any magnetic field and therefore it may display a paramagnetic structure. For deformability parameter values close to one, our model describes a magnetic compound for which the deformability effects tend to encumber that of the applied magnetic field.

Case 2. For values of r tending to -1, we recover once more a Heisenberg model Hamiltonian with a planar anisotropy, but here with the difference that there is an additional term, which is denoted as H_{def} and reads $H_{\mathrm{def}} = 2g\mu_{\mathrm{B}}B_x SN$. This expression just shifts the energy of the system without any influence either on the dynamics or on the stability of the system under modelization. In the context of a system that displays an intrinsic magnetic gap, this Hamiltonian limit can be very useful because this gap can be absorbed or cancelled by the residual fundamental magnetic energy. This situation is always found in ferrimagnets with a great tendency to ferromagnetic order.

Case 3. When $r = 0$, the last term of equation (2.14) becomes $H_{\mathrm{def}} = g\mu_{\mathrm{B}}B_x \sum_i (S - S_i^x)$. In this last term we notice the presence of the ground state energy and the Zeeman energy. Hence, from our deformable model, when the deformability parameter vanishes, we recover the Heisenberg model with Zeeman energy and a planar anisotropy in addition to a ground state energy. Fundamentally the presence of the ground state energy here does not matter because it has no influence, either on the magnetic structure or on the spin dynamic stability.

This Hamiltonian, then, turns out to be more suitable because it allows study of the dynamics of a wide range of ferromagnetic and antiferromagnetic systems that belong to the class of the 1D model. It also appears as a sort of interpolation between an Ising model and a planar Heisenberg model.

2.1. Equations of motion

As mentioned above, the framework of our present considerations here is the classical spin theory where the spins are usual three-dimensional (3D) vectors $\vec{S}_i$ of constant length S, i.e. neglecting quantum effects ($\frac{A}{JS(S+1)} \ll 4\pi^2$) [5, 20]. In classical notation, we represent the spin field in spherical coordinates, i.e. as given in equation (2.3), with angles in the ranges $0 \leqslant \theta_i \leqslant \pi$ and $0 \leqslant \varphi_i \leqslant 2\pi$.

Then, using the undamped Bloch equations for the spin vectors,

$$\hbar \frac{\mathrm{d}\vec{S}_i}{\mathrm{d}t} = \vec{S}_i \Lambda \vec{F}_i \tag{2.15}$$

with the relation

$$\vec{F}_i = -\frac{\partial H}{\partial \vec{S}_i} \tag{2.16}$$

for the effective field, we have that

$$\vec{F}_i = J(\vec{S}_{i+1} + \vec{S}_{i-1}) - 2AS_i^z\vec{e}_z + \frac{g\mu_{\mathrm{B}}SB_x(1-r^2)\vec{e}_x}{(1+r^2+2rS^{-1}S_i^x)^2}. \tag{2.17}$$

Here, $\vec{e}_x$ ($\vec{e}_z$) is the unit vector along the X axis (the Z axis). While $\vec{F}_i$ represents the effective field acting on each spin, the expression $\vec{S}_i \Lambda \vec{F}_i$ represents the torque on the spin at lattice site i, respectively. Therefore, after some mathematical combinations between the spherical spin coordinate and equations (2.17) with (2.15), the equations of motion are [22, 24, 32–34]

$$\frac{\hbar}{JS}\frac{\mathrm{d}\varphi_i}{\mathrm{d}t}\cos(\theta_i) = \sin(\theta_i)[\cos(\theta_{i+1})\cos(\varphi_{i+1}-\varphi_i)+\cos(\theta_{i-1})\cos(\varphi_{i-1}-\varphi_i)] - \cos(\theta_i)[\sin(\theta_{i+1})+\sin(\theta_{i-1})] + \frac{2AS}{J}\cos(\theta_i)\sin(\theta_i) + \frac{g\mu_{\mathrm{B}}B_x}{JS^2}\frac{(1-r^2)^2\sin(\theta_i)\cos(\varphi_i)}{[1+r^2+2r\cos(\theta_i)\cos(\varphi_i)]^2} \tag{2.18a}$$

$$\frac{\hbar}{JS}\frac{\mathrm{d}\theta_i}{\mathrm{d}t} = \cos(\theta_{i+1})\sin(\varphi_{i+1}-\varphi_i)+\cos(\theta_{i-1})\sin(\varphi_{i-1}-\varphi_i) - \frac{g\mu_{\mathrm{B}}B_x}{JS^2}\frac{(1-r^2)^2\sin(\varphi_i)}{[1+r^2+2r\cos(\theta_i)\cos(\varphi_i)]^2}. \tag{2.18b}$$

The set of coupled nonlinear differential-difference equations (2.18*a*) and (2.18*b*) defines the collective excitations for the in-plane angle φ_i and the out-of-plane angle θ_i of a discrete lattice. It is extremely difficult to perform a complete analysis of the system of equation (2.18) analytically. Therefore, only a numerical simulation can allow a detailed study of the topological solitons travelling in the system. For this purpose, we first need to carry out some calculations in the continuum limit.

2.2. Analytical solution in the continuum limit

While the model under study is discrete, it is important to derive the continuum limit because it helps in establishing the analytical calculation of the implicit soliton solutions that would be used as initial conditions for our numerical computation. Using then the classical approximation at sufficiently low temperature ($T < (AJ)^{1/2}$), in the continuum limit (where the length scale rotation $JS/g\mu_{\mathrm{B}}B_x \gg 1$), equations (2.18*a*) and (2.18*b*) can be reduced to the following partial nonlinear coupled differential equations:

$$\varphi_\tau\cos\theta = -\theta_{\eta\eta} + (1-\varphi_\eta^2)\sin\theta\cos\theta + b(1-r^2)^2\frac{\sin\theta\cos\varphi}{[1+r^2+2r\cos\theta\cos\varphi]^2} \tag{2.19a}$$

$$\theta_\tau = -\varphi_{\eta\eta}\cos\theta - 2\theta_\eta\varphi_\eta\sin\theta - b(1-r^2)^2\frac{\sin\varphi}{[1+r^2+2r\cos\theta\cos\varphi]^2}. \tag{2.19b}$$

In these equations, we have introduced the dimensionless quantities $\eta = \sqrt{\frac{2A}{J}}\frac{Z}{a}$ (where a is the lattice spacing), $\tau = (\frac{2AS}{\hbar})t$ and $b = \frac{g\mu_{\mathrm{B}}B_x}{2AS}$. The sine–Gordon approximation can then be obtained at the order ε^2 if $\frac{\partial}{\partial\eta}, \frac{\partial}{\partial\tau} \sim \varepsilon(\varepsilon \ll 1)$ (which corresponds to the continuum approximation for permanent profile solutions), $\theta \sim \varepsilon$ and $b \sim \varepsilon^2$.

Equations (2.19*a*) and (2.19*b*) then reduce to

$$\varphi_{\eta\eta} - \varphi_{\tau\tau} - b(1-r^2)^2\frac{\sin\varphi}{[1+r^2+2r\cos\varphi]^2} = 0 \tag{2.20a}$$

$$\theta = \varphi_\tau. \tag{2.20b}$$

Here, b and r are the two constants needed to specify the time evolution of the spin excitations. It is therefore obvious to see that the last term of equation (2.20*a*) is the first derivative with respect to φ of the Remoissenet–Peyrard potential (RP) [38, 39] given in equation (2.11). Equation (2.20*a*) is the well known deformable sG equation; it has solutions in the form of large amplitude travelling waves (kinks), low amplitude linear modes (spin waves or magnons) and breathers [38, 39]. This equation also shows that in this approximation the ferromagnetic solitary excitations are composed of two families of implicit kink solutions, with the velocity v given in terms of moving coordinate $\xi = \eta - v\tau$, which are travelling wave rotations of the spin through 2π within the easy plane. Under this assumption, equation (2.20*b*)

informs us on the fact that the spin tilt out of the easy plane will be proportional to the kink translation velocity. The implicit solutions are [38, 39]

$$\frac{\gamma\xi}{d^{(1)}} = \operatorname{sgn}(\varphi-\pi)\left\{\frac{(1-\alpha^2)^{\frac{1}{2}}}{\alpha}\tan^{-1}\left[\frac{(1-\alpha^2)^{\frac{1}{2}}}{(\alpha^2+\tan^2(\varphi/2))^{\frac{1}{2}}}\right]+\tanh^{-1}\left[\frac{\alpha}{(\alpha^2+\tan^2(\varphi/2))^{\frac{1}{2}}}\right]\right\} \tag{2.21a}$$

with the rest energy

$$E_s^{(1)} = 8A'\sqrt{b}\alpha(1-\alpha^2)^{-\frac{1}{2}}\tan^{-1}\left[\left(\frac{1-\alpha^2}{\alpha}\right)^{\frac{1}{2}}\right] \qquad \text{for } -1 < r \leqslant 0 \tag{2.21b}$$

and

$$\frac{\gamma\xi}{d^{(2)}} = \operatorname{sgn}(\pi-\varphi)\left\{(1-\alpha^2)^{\frac{1}{2}}\tanh^{-1}\left[\frac{(1-\alpha^2)^{\frac{1}{2}}}{(1+\alpha^2\tan^2(\varphi/2))^{\frac{1}{2}}}\right] - \tanh^{-1}\left[\frac{1}{(1+\alpha^2\tan^2(\varphi/2))^{\frac{1}{2}}}\right]\right\} \tag{2.21c}$$

with the rest energy

$$E_s^{(2)} = 8A'\sqrt{b}\alpha(1-\alpha^2)^{-\frac{1}{2}}\tanh^{-1}\left[\left(\frac{1-\alpha^2}{\alpha}\right)^{\frac{1}{2}}\right] \qquad \text{for } 0 \leqslant r < 1 \tag{2.21d}$$

and

$$\alpha = \frac{1-|r|}{1+|r|} \tag{2.21e}$$

$$d^{(1)} = d_0\alpha, \qquad d^{(2)} = d_0/\alpha, \qquad d_0 = \frac{1}{\sqrt{b}}, \qquad A' = \frac{\hbar^2}{2Aa} \qquad \text{and} \qquad \gamma = (1-v^2)^{-1/2}. \tag{2.21f}$$

The out-of-plane component remains defined by equation (2.20*b*) for both of the implicit in-plane solutions.

Let us mention that, since the Remoissenet–Peyrard potential presents more than two harmonics [38], such a model can be applied to a bi-layer film of Ni/Pd, for which Tsukamoto *et al* [40] have shown by molecular dynamic analysis that the perpendicular magnetic anisotropy is related to the amount of stress in each Ni layer, and consequently the distribution potential between two sites on an fcc(111) and an fcc(100) surface presents a shape with many harmonics. In the case of the Fe/Cr (211) superlattice system that is isomorphic to a classical two-sub lattice uniaxial antiferromagnet, the intrafilm interaction keeps all the spins belonging to the same film parallel to each other. Then, a single layer can represent each film. Hence, the determination of the ground state of the three-dimensional superlattices reduces to a one-dimensional problem in the direction normal to the film surfaces. Therefore, the Hamiltonian that is defined by equation (2.14) becomes suitable not only for the well studied $CsNiF_3$ material [5], but also for such a system.

Since the validity of the continuum limit and other approximations, however, can only be tested by comparison with numerical calculations, we are left with a central question of the physical problem described by the discrete non-integrable system of equations (2.18*a*) and (2.18*b*) for our magnetic chain, namely: what is the signature of the implicit soliton solution on the dynamics of the magnetic chain for different values of the parameter r.

3. Numerical experiments

In this section, we present the results of a numerical experiment in a discrete deformable magnetic chain. The validity of the analytical result obtained from the continuum approximation is discussed in detail. In order then to investigate the dynamics of a single implicit kink soliton, as well as its collision with other kinks and antikinks, we are going to solve numerically the set of coupled nonlinear differential-difference equations of motion (2.18*a*) and (2.18*b*). These coupled differential-difference equations are a consequence of the presence of a second degree of freedom θ. In such a system, the role of the second component may be affected by the strength of the magnetic field. We will show to what extent the properties of the one-component soliton model are preserved in a two-component magnetic system.

3.1. Computer-simulation details

Our numerical calculations have been done through a computer-simulation program to study the dynamics of the implicit kink (antikink) soliton on a cyclic magnetic chain which is constituted of 160 spins. In physical application, a minimum distance scale that leads to discreteness effects naturally occurs (e.g. lattice constant). Therefore, in these simulations, the degree of discreteness is controlled by the ratio $\gamma/d^{(i)}$ (where $i = 1, 2$), and $d^{(i)}$ is also a function of the reduced magnetic field and the parameter r (see equations (2.21*e*) and (2.21*f*)). In order to control the discreteness effect arising from the system, for a given velocity, we chose particular values of the parameter $d^{(i)}$. For instance, in some cases the physical parameters that can induce the discreteness effects were chosen in order to keep the implicit static soliton width in a range of 10–20 spins during the complete run. Let us introduce, as an example, the following set of parameters of the $CsNiF_3$ structure, namely [13] $J = 23.6$ K, $A = 4.5$ K and $S = 1$. In addition, working with the cyclic magnetic chain presupposes that we chose periodic boundary conditions and an offset of 2π at chain ends is needed.

As far as equations (2.18*a*) and (2.18*b*) are concerned with the description of the subsequent time evolution of the in-plane and the out-of-plane excitations, the origin of the energy scale of our discrete ferromagnetic chain is chosen from the uniform ferromagnetic state. Its dimensionless form is given in terms of the in-plane and the out-of-plane angle components by $E = \sum_i E_i$, with

$$\begin{aligned} E_i = {} & 1 - \cos(\theta_i)\cos(\theta_{i+1})\cos(\varphi_{i+1} - \varphi_i) - \sin(\theta_i)\sin(\theta_{i+1}) \\ & + 1 - \cos(\theta_i)\cos(\theta_{i-1})\cos(\varphi_{i-1} - \varphi_i) - \sin(\theta_i)\sin(\theta_{i-1}) \\ & + a_2\frac{\sin^2(\theta_i)}{2} + a_3(1-r)^2\frac{1 - \cos(\theta_i)\cos(\varphi_i)}{(1 + r^2 + 2r\cos(\theta_i)\cos(\varphi_i))} \end{aligned} \tag{3.1}$$

where $a_2 = \frac{2A}{J}$, $a_3 = \frac{g\mu_B B_x}{JS}$ and the index (i) stands for the lattice sites. With a suitable choice of the time step, this energy is a conserved quantity. Therefore, as in [35], it was frequently monitored in our simulations to insure an accuracy of about 0.01% for the fourth-order Runge–Kutta scheme.

The initial conditions, which are typically at time $t = 0$, and initial profiles of the in-plane and the out-of-plane component of the spin deviation are obtained by using the implicit solutions (see equations (2.21)).

For the numerical implementation of these implicit solutions, the Newton–Raphson scheme, which is the approach used by Remoissenet and Peyrard [38], or a pseudo-spectral approach can be chosen [41]. However, these approaches seem to be limited because these methods remain just an approximation. We used a direct method instead and it turned out to represent a 2π-kink soliton when $r = 0$ more accurately. To this end, once we have the

velocity v, we next define a set of discrete values of the in-plane component in such a way that the interpolation points of lines are given by

$$\varphi_i = \frac{2\pi \mathrm{i}}{N} \tag{3.2}$$

with $i \in [0, \ldots, N]$ and $N = 160$ the spin–lattice size. We then use this definition of φ_i in the discrete version of equations (2.21a) and (2.21c) given by

$$\xi_i = \operatorname{sgn}(\varphi_i - \pi)\frac{d^{(1)}}{\gamma}\left\{\frac{(1-\alpha^2)^{\frac{1}{2}}}{\alpha}\tan^{-1}\left[\frac{(1-\alpha^2)^{\frac{1}{2}}}{(\alpha^2+\tan^2(\varphi_i/2))^{\frac{1}{2}}}\right] + \tanh^{-1}\left[\frac{\alpha}{(\alpha^2+\tan^2(\varphi_i/2))^{\frac{1}{2}}}\right]\right\} \tag{3.3a}$$

for $-1 < r \leqslant 0$ and

$$\xi_i = \operatorname{sgn}(\pi - \varphi_i)\frac{d^{(2)}}{\gamma}\left\{(1-\alpha^2)^{\frac{1}{2}}\tanh^{-1}\left[\frac{(1-\alpha^2)^{\frac{1}{2}}}{(1+\alpha^2\tan^2(\varphi_i/2))^{\frac{1}{2}}}\right] - \tanh^{-1}\left[\frac{1}{(1+\alpha^2\tan^2(\varphi_i/2))^{\frac{1}{2}}}\right]\right\} \tag{3.3b}$$

for $0 \leqslant r < 1$.

Equations (3.2), (3.3a) and (3.3b) allow us then to recover, for each amplitude of φ_i, its corresponding localization on the lattice site ξ_i, for different values of the deformability parameter. At this step we shall reiterate that the out-of-plane component is defined by

$$\theta_i = \frac{\mathrm{d}\varphi_i}{\mathrm{d}t} = -v\frac{\mathrm{d}\varphi_i}{\mathrm{d}\xi_i}. \tag{3.4a}$$

Therefore, it can be numerically extracted through the following relation:

$$\theta_i = -v\frac{\varphi_{i+1} - \varphi_{i-1}}{(\xi_{i+1} - \xi_{i-1})} \tag{3.4b}$$

where v represents the reduced effective velocity of the soliton moving in the spin–lattice. Therefore, in the present simulation, we are able to test the validity of the implicit solutions through their propagation in the discrete chain for different values of the parameter r and the reduced magnetic field b.

3.2. Outcome of the analytical solutions in the discrete deformable spin chain

In this section we present results of numerical treatment in the case of both strong and weak coupling between neighbouring spin so that the continuum approximation is either valid or not. When the continuum approximation is valid, the system exhibits a free-kink propagation scheme with a shape that is very close to the initial profile. However, when it is not valid, the topological soliton involving in the spin–lattice may then present either a splitting shape while moving or a kink moving with an oscillating background for the in-plane component, while the shape of the out-of-plane component displays a breather shape instead of a simple pulse of the initial conditions.

3.2.1. Magnetic solitary wave stability limit. Magyari *et al* [25, 26] have shown that magnetic solitons have a reduced stability range with respect to standard sine–Gordon solitons. There exists a critical magnetic field above which they become unstable. We have tested numerically the conditions of existence of solitons in the deformable model. They are summarized in

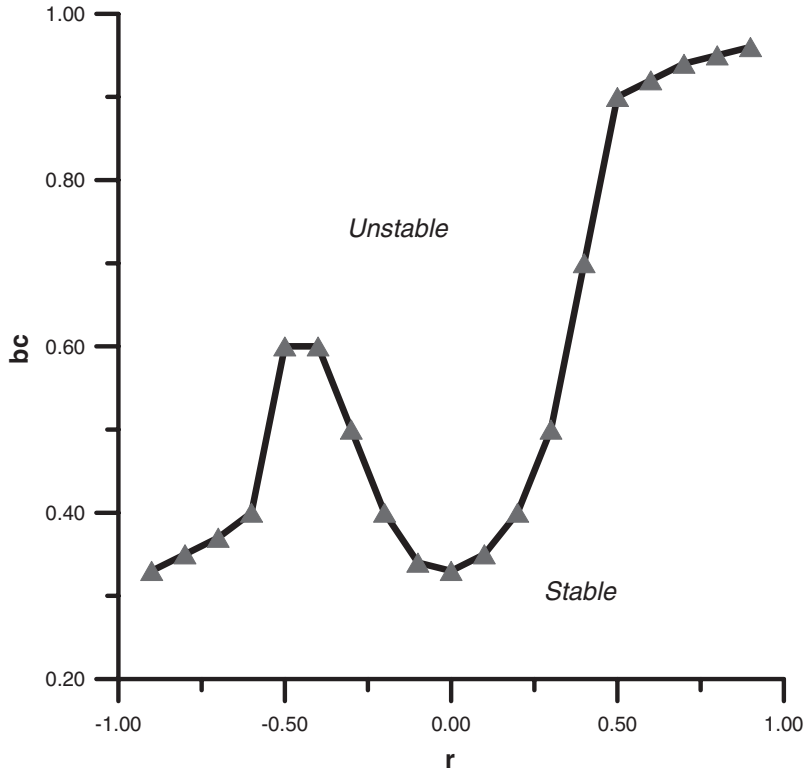

Figure 1. Stability diagram where the critical reduced magnetic field b_c is plotted as a function of the deformability parameter r in the range $-1 < r < 1$. It displays the region of stability of solitary waves. Here the initial conditions are based on the analytical solution of the continuum approximation with an initial velocity that should not exceed $v = 0.5$ for $r > 0$ and $v = 0.75$ for $r < 0$.

figure 1 where a stability diagram is set up. From this figure obtained with the $CsNiF_3$ material parameters, we observe that, when $r > 0$, the critical value of the reduced magnetic field increases with increasing deformability parameter up to a value of $b_c = 0.96$ for $r = 0.9$. For $r < 0$, this critical value also increases with reducing values of the deformability parameter but after the value of the shape parameter $r = -0.5$, where it reaches the value of the reduced critical magnetic field of $b_c = 0.6$, it starts decreasing to a value of $b_c = 0.33$ for $r = 0.9$ that also corresponds to the critical value of the reduced magnetic field when $r = 0$. This decreasing value of b_c when $r < -0.5$ can be understood in the sense that, in this range of parameter, it happens that the system displays strong discreteness effects whenever the discreteness parameter is monitored. But, due to the fact that the minimal value of b_c when r is negative remains equal to the case of $r = 0$, the range of stability remains increased. Finally, it is clear from this figure that one of the main effects of the deformability is to induce a larger range of the reduced magnetic field for the existence of the solitary waves. Therefore, depending on the final shape of the magnetic solitons when the deformability is considered in a (1D) Heisenberg chain, the range of their stability while propagating is considerably enhanced. It is worth mentioning that for positive values of r, to increase the range of stability, it was necessary to use initial conditions with velocity not higher than $v = 0.65$. For greatest velocities, the motion of the soliton slows down. Their instability is obtained for the highest

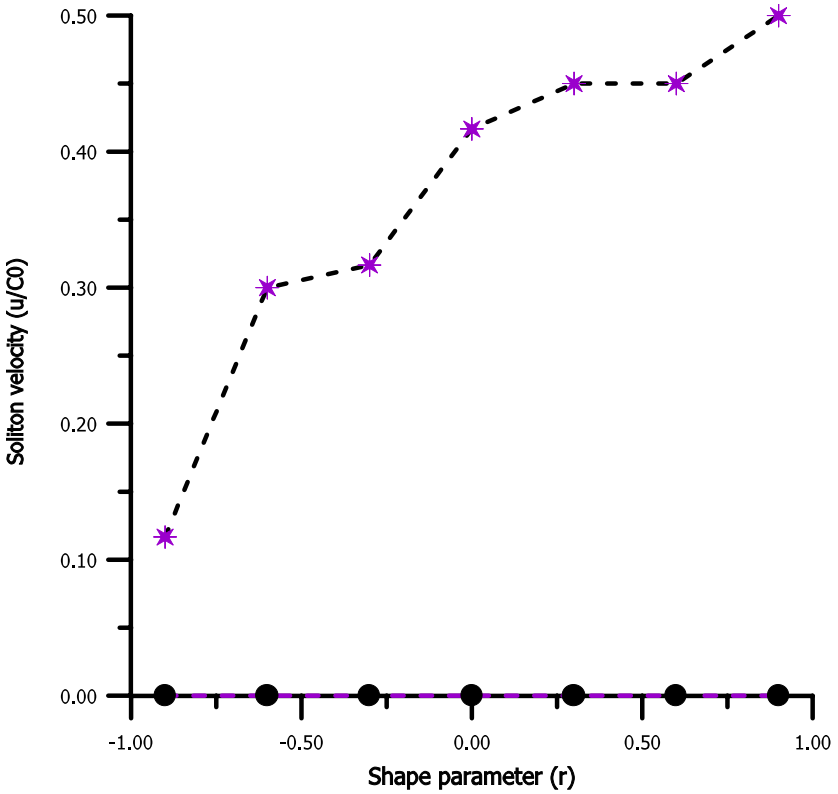

Figure 2. Maximum and minimum mean propagation velocity of the resulting soliton against the deformability parameter (r) for all the reduced magnetic field with range [0, 0.61]. Here we proceeded in our simulation by computing, for a given value of the deformability parameter, all the velocities of the solitary waves for all the values of the magnetic field. For a given magnetic field we let the initial condition propagate for all values of initial velocities in the range of $0 < v < 0.9$. At the end we retained both the maximal and the minimal velocity. Next we increase the magnetic field and restart the process in order to come out only with the maximal and the minimal value of the effective soliton velocity for a given value of r.

magnetic field. Thus, the system intrinsically selects the velocity of the magnetic soliton propagating in the chain.

3.2.2. Free kink and splitting kink propagation. As we can observe in the stability diagram of figure 1, there exists a large range of the deformability parameter r for which the in-plane component propagates for a very long time without a sensible change from its initial profile. Only the out-of-plane component may propagate with a slight radiation of magnons in the lattice. This tendency to long life of the wave propagating in the chain is a good indication of a possible great stability of the kink in our deformable magnetic spin system; this is possible even for very large values of the magnetic fields compared to those allowed for a rigid magnetic chain. In figure 2, we plotted the maximal value and the minimal value of the effective velocity of the propagating wave as a function of the deformability parameter (r) for all the reduced magnetic field (b) in the range $0 \leqslant b \leqslant 0.61$. From the schematic plot of figure 2 it follows that the discrete system of equations (2.18a) and (2.18b) admits a moving kink solution with constant profile for each value of the deformability parameter (r), and the reduced applied

magnetic field (b). These moving solitons display a finite interval for the effective velocity that varies from a minimal value of zero, which corresponds to the points on the abscissa axis of the shape parameter (r), to a maximal speed with range [0.1, 0.5] given on the upper curve. Thus, in these conditions the implicit kink (see equations (2.21)) solution used as initial condition seems to represents good solution of a discrete lattice. From figure 2, we also found that the effective speed of the solitary waves propagating increases with increasing shape parameter. This can be understood in the sense that the kink profile is smoother when r tends to unity; in contrast it has sharp angles when r tends to -1. This then suggests that the maximal effective velocity is influenced by the discreteness effect. It is also interesting to note that if we introduce the ideal sine–Gordon kink as an initial condition we will obtain the same result as Peyrard and Remoissenet [39] in the case of a deformable atomic lattice. Here also, the shape of the kink will progressively turn to that of the implicit soliton solution (see equations (2.21)) with small amplitude oscillations but, as we mentioned in [35], the highest values that can be attained by the out-of-plane component do alter the stability of this kind of kink.

For all the deformability parameters, when the reduced applied magnetic field (b) is in the range $0 \leqslant b < 0.1$, then as soon as the initial condition is introduced in the chain it rapidly transforms to a bi-kink shape that is really two kinks that are linked and, thus, moving in opposite directions. It also follows from our simulations that, depending on the value of the deformability parameter, the sizes of the two kinks can be equal or different. When the sizes of two kinks are equal, the 2π bi-kink, while propagating, exhibits a two-π-kink motion scenario, which is equivalent to an elastic collision that is produced in the middle of the chain and, due to a periodic boundary condition, also at the chain's end. This can be seen in figures 3(a) and (b) where we have plotted the in-plane component as well as the out-of-plane component of the spin wave propagating with a transparent collision motion, which is produced as a mutual crossing. Figure 3(c) is a schema that illustrates very well the mutual crossing of the two excitations engaged in the collision process. The contour plot of the time against the position shows that it happens both at the chain's end for the first time and the next time at its middle and the processes continue in the same order, while the entire 2π-kink moves progressively. However, when the sizes of the two sub-kinks are different, the same transparent collision motion is produced but at different spin–lattice sites situated between the middle and the end of the chain. We also noted in this latter case that the kink with greater size was more rapid than the other one. Therefore, it was possible to find collision processes repeated many times on the same side of the chain before changing. Figures 4(a) and (b) are shown to illustrate these collision processes that happen when the in-plane component and the out-plane spin tilting are propagating in the lattice. This multiple collision exhibited on the same side is well illustrated in figure 4(b) where the out-of-plane component moves. Here, the wave represented by the reversed pulse shape is faster than the wave represented by the upper pulse shape. Physically, these multiple collisions exhibited by the sub-kink that arises in this range of parameters is the consequence of the fact that the system displays an internal mode. This is the proof that the property of the internal mode that is found in the dynamics of the one-component deformable soliton model [38, 39] is also present in that of a deformable magnetic system where two degrees of freedom are coupled.

3.2.3. Moving solitons on an oscillating background (nanopteron). In the study of the interaction of a kink with small amplitude waves, several different behaviours can be identified theoretically and numerically depending on whether we are in the continuum limit approximation or we are taking into account lattice effects.

(i) Linear kink stability analysis reveals that there will be at least one bound state, representing rigid translation of the kink (Goldstone mode). There may be further finite frequency

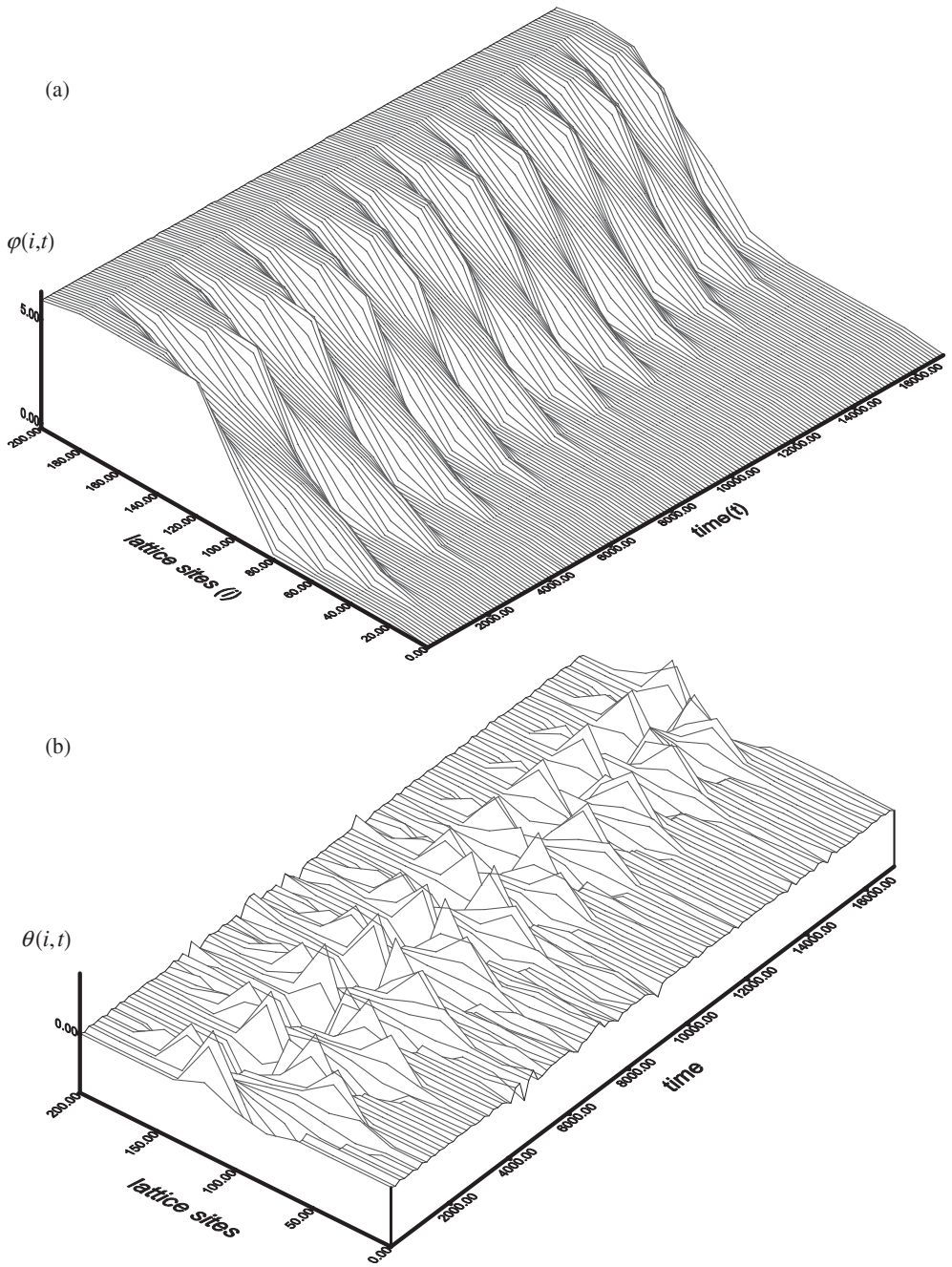

Figure 3. Computer generated motion both for the in-plane (a) and out-of-plane (b) solitary waves governed by the original discrete system of equations (2.5*a*) and (2.5*b*) for the deformability parameter ($r = -0.9$) and the reduced magnetic field $b = 0.013$ with the initial velocity $v = 0.52$. (c) The contour plot of the position of the two excitations engaged in the collision process against time. The solid curve corresponds to the trajectory of the excitation initially positioned on the left-hand side of the centre of the chain, while the broken curve corresponds to the second excitation initially positioned on the right-hand side of the spin–lattice.

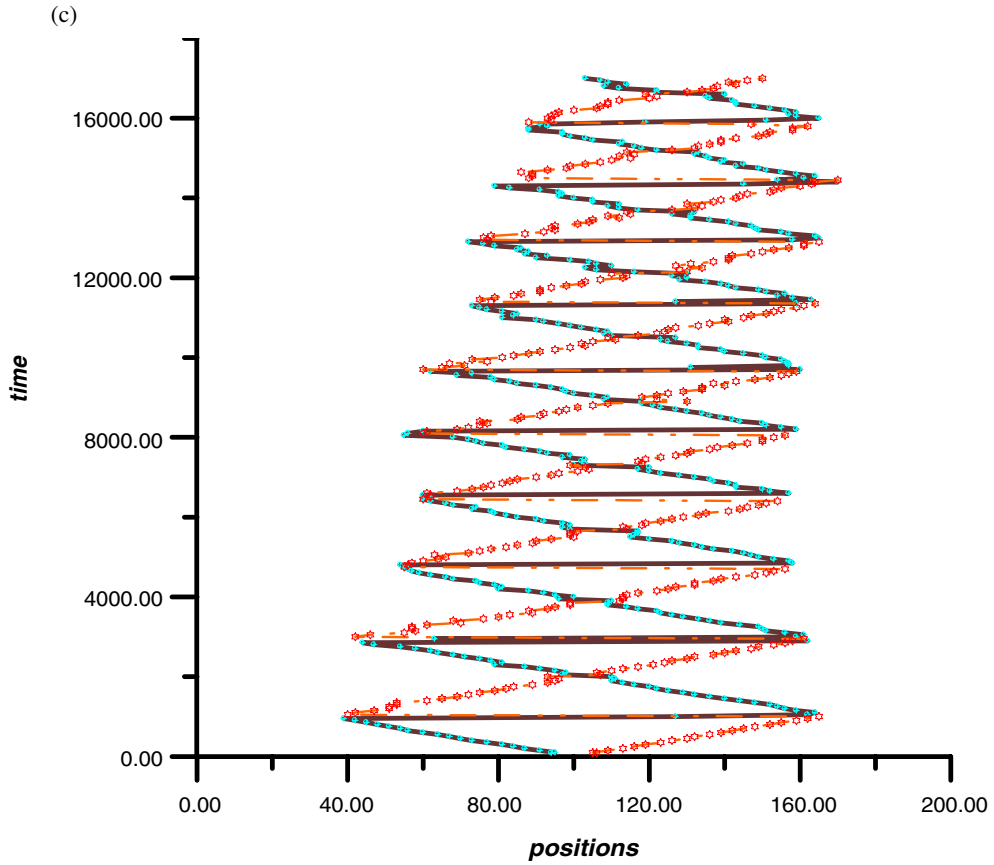

Figure 3. (Continued.)

bound states describing localized kink oscillations. In addition, there will be a scattering (kink-phonon) continuum. In fact, for sine–Gordon or ϕ^4, the scattering problem is purely reflectionless: the phonon dispersion is unchanged by the presence of a kink, whose only effects are to produce an asymptotic phonon phase shift which depends on the velocity of wave propagation [42, 43].

A number of computer simulations and theoretical studies have been made on the importance of discreteness effects on the structural and dynamical properties of sine–Gordon and ϕ^4 chains. More recently, it has been shown that the discreteness effects that are known to exist for topological solitons also exist for non-topological kink solitons in nonlinear lattices.

(ii) Discreteness effects can lead to the damped oscillatory motion and the lattice pinning effects (Peierls–Nabarro (PN) potential) of topological solitons, the adiabatic dressing of kinks and the spontaneous emission of phonons [44, 45].

(iii) Supersonic solitons in monatomic chains can propagate at constant speed even if they are very narrow and if they have very large amplitude. Unlike topological solitons, they do not radiate any small amplitude oscillation and exhibit soliton-like properties even if their width is of the order of the lattice spacing. However, numerical simulations have shown a small energy loss when they collide [46].

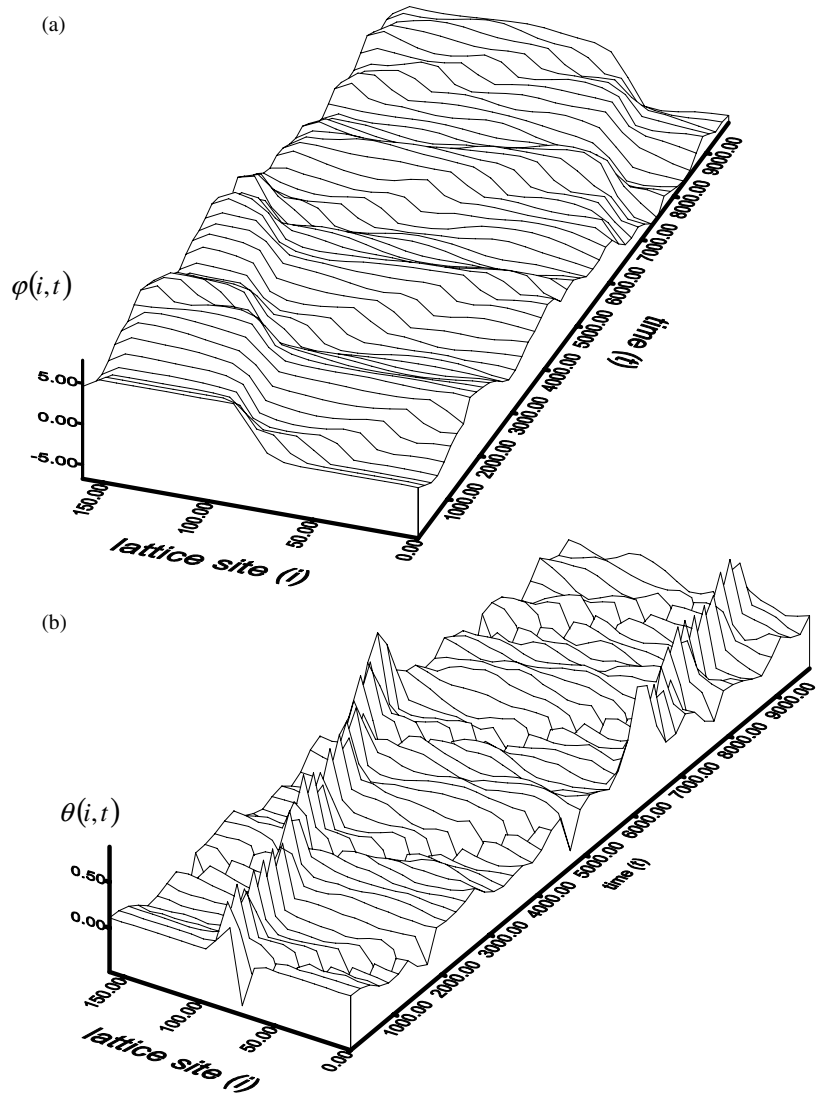

Figure 4. Plot of the time development of an exact solution of the continuum equation of motion in the discrete spin for $b = 0.03$ and $r = 0.4$ and the velocity of the initial condition $v = 0.5$. (a) In-plane component motion. (b) Out-of-plane component motion.

(iv) It has been also demonstrated, by numerical simulations, that the permanent radiation of small amplitude oscillations is an essential characteristic of narrow subsonic solitons in a monatomic lattice [46].

(v) Solitons in a diatomic chain exhibit discreteness effects, whatever their velocity, due to the existence of an optical branch in the linear dispersion relation of such a lattice. Consequently, a diatomic lattice cannot sustain narrow kinklike excitations with soliton properties because they always lose energy by radiating optical oscillations [46].

(vi) Kinks propagate preferentially at well defined velocities which correspond to quasi-steady states, while a kink moving at other velocities suffers relatively high rates of radiation of small amplitude oscillation [31].

(vii) By moving solitons on an oscillating background we mean waves that propagate with a bound state of a self-trapped kink and a small amplitude wave with a nonlinear dispersion law. When such waves move in our spin–lattice, the scenario exhibited by the nonlinear excitation while propagating is that of a kink pinned to the (nonlinear) wave that decreases its velocity (see figure 5(a)), and finally it turns out that this wave forces the kink to propagate in a coupled way, i.e., some kind of dynamical self-trapping mechanism of the resulting kink with the nonlinear wave. Figure 5(b) is a schema that illustrates the kink profile of the in-plane component propagating with an oscillating tail, which is the so-called 'nanopteron'. A nanopteron is a permanent but non-local and spatially extended soliton whose spatial radiation can only be minimized but not eliminated [47]. Otherwise, whenever it could suffer from an exponential decay, it should happens very far away from the kink. Here, the soliton motion occurs on a background of a nonlinear modulated and oscillating wavetrain that can allow the kink to propagate in the discrete spin chain with any constant subsonic velocity (see figure 5(a)), whenever the Peierls–Nabarro barrier exists. The presence of the nanopteron is coherent with the one-component soliton model [41]. The existence of the radiation effects is noticeable for r approaching -1 with higher values of the reduced magnetic field and disappears when r approaches the value 1. It is also worth mentioning that this nonlinear wave appears with a small amplitude of $A = 0.06$ in dimensionless units with a multi-periodic shape constituted of a period for the rapid oscillation and a period for the bumps that map the wavetrain's shape.

3.3. Collision process of the solitons in the discrete deformable spin chain

We are mainly interested in the properties of a 2π-kink (or a 2π-antikink) when they collide in order to determine their stability in a ferromagnetic chain under deformability effects. In order to study the collisions of the in-plane and out-of-plane moving soliton components of the spin deviations, we simulate the system of equation (2.18) with periodic boundary conditions for the chain consisting of $N = 200$ spins. Using boundary conditions here is important because it helps to avoid end effects. We still use the fourth order Runge–Kutta method with the same accuracy as required for the single-soliton propagation. We choose initial conditions in the same way as in the case of the single soliton; i.e., here we take a pair of the implicit kink (or antikink) for the in-plane component and the derived pulses for the out-of-plane component with opposite velocities from equations (2.21a) and (2.21c) and (3.4), respectively. In these conditions the two solitary waves move towards each other for two spin components.

3.3.1. Head-on collision between a 2π-kink and a 2π-kink. When the two solitary waves of 2π-kink type are involved in such a magnetic chain with the same velocities, if they are displayed in opposite directions, they start by moving towards each other. Then, we observed that the final state can be either dependent or not on the initial energy of the two excitations. Depending on the range of the shape parameter (r), each of the two 2π-kinks faces either a repulsive interaction or an attractive one. Three processes allowed for these collisions are dictated by the parameter r. The two waves of 2π-kink type can pass through each other, or be reflected elastically or non-elastically, or else they can form a standing or a nonstanding bound state. For different values of the deformability parameter (r) with range $]-1, \ldots, 0.4]$, whatever the initial velocity chosen for a reduced magnetic field greater than $b = 0.33$, the collision of the solitary waves of 2π-kink profile results in a strong inelastic interaction. The scenarios displayed here by the two excitations consist of a completely destroyed shape when they collide for the 2π-kink of the in-plane, but for the particular value of $b = 0.33$ and

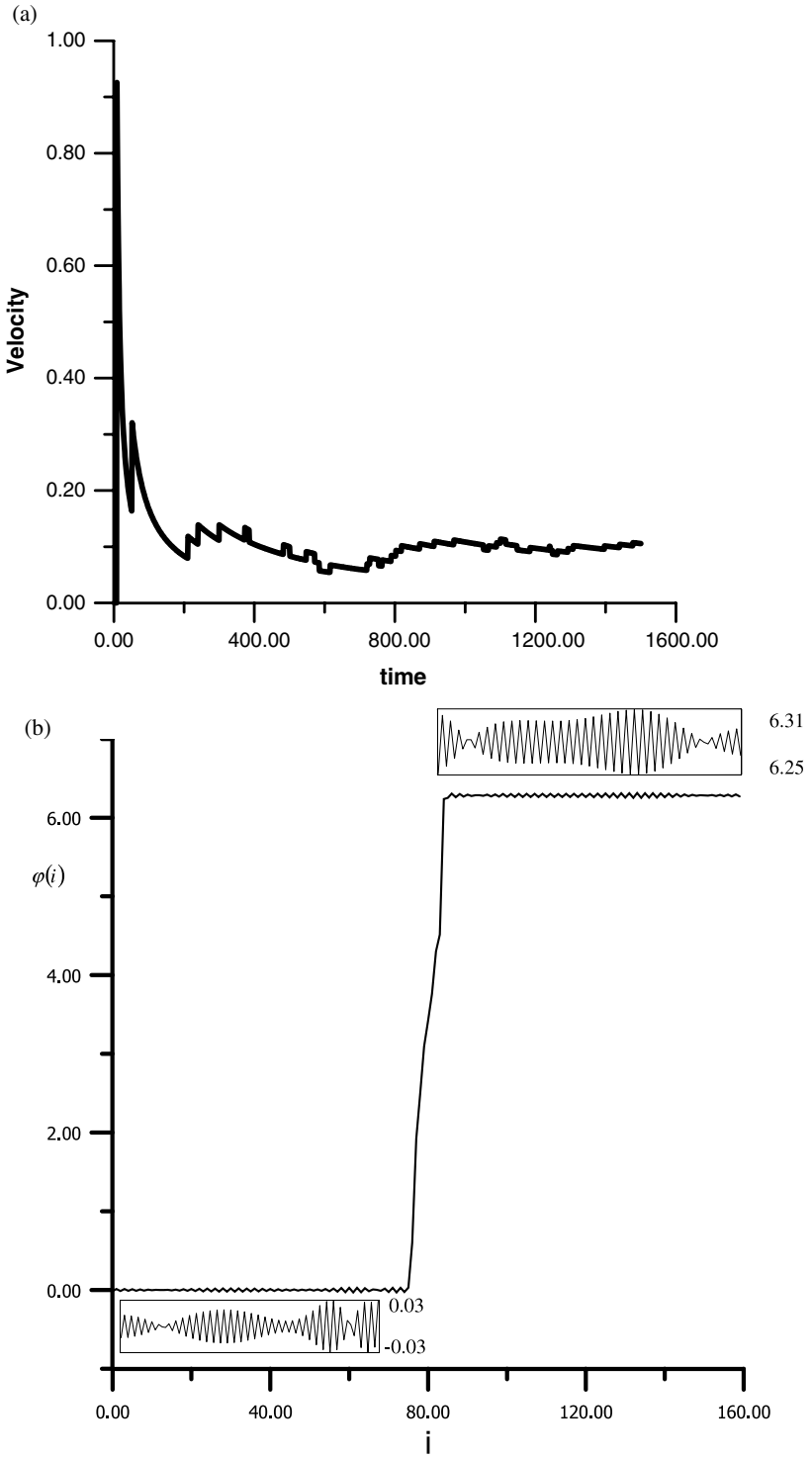

Figure 5. (a) Plot of the velocity of the nanopteron wave as a function of time showing a decreasing behaviour that progressively tends to a constant value. (b) Plot of the shape of the nanopteron for the in-plane component of the spin moving in a spin chain for the parameters $r = -0.8$, $b = 0.32$ and velocity $v = 0.74$.

$r = 0.4$, while the 2π-kink shape is destroyed by the collision process, the resulting breathers of the out-of-plane component face a mutual crossing with just slight radiation. Therefore, in these ranges of parameters the system can support long time moving 2π-kink solitary waves but without particle-like properties. For us, this is the signature of the fact that within these parameter ranges the system does not admit a 2π-kink soliton solution and therefore it is not integrable, but may be nearly integrable. When the deformability parameters with range $]-1, 1[$ are used, for all reduced magnetic fields in the range $0 \leqslant b \leqslant 0.33$, the collision scenarios displayed by the two excitations correspond to a mutual crossing of each other (see figures 6(a) and (b)). We notice from figure 6(b) that the out-of-plane component moves with breather shapes instead of a simple pulse of the initial condition. The mutual crossing phenomenon displayed by the two excitations is a good indication of the fact that, in this range of parameters, the system appears to be integrable since the solitons' robustness is proved by the elastic collision process whenever their final shapes are different from those of the initial conditions. Moreover, for the reduced magnetic field greater than $b = 0.33$, the mutual crossing happens only for $r \geqslant 0.7$, while for the values of r with range $]0.4, \ldots, 0.7[$, we observed most of the time an elastic reflection of the two excitations engaged in the collision process. However, we found an unexpected scenario for the deformability parameter $r = 0.6$ and the reduced magnetic field $b = 0.21$, which behaves as a three-particle interaction resulting from the collision process. Here we noted the presence of a nonlinear wave that helps to keep a minimum distance between the two excitations of 2π-kink type. It then engages itself in the collision processes after the first collision between the first two excitations. Here the motion of the nonlinear wave is equivalent to that of an elastic string that is embedded between the two kinks (antikink) and therefore it is subjected to compression or an extension of its length during the collision. In figure 6(c), which is shown to illustrate this new phenomenon, we observed that as soon as the initial conditions representing the two excitations are introduced in the magnetic chain, they suddenly move toward each other and then, rapidly, the first collision happens at time $t = 3000$. After that, an interaction of three-particle type is engaged as long as the simulation process remains, with the domination of the compression and the extension of the nonlinear wave, which intercalate between the resulting 2π-kinks. For instance, the second extension, when the repulsive phenomenon dominates, happens between $t = 12\,000$ and 20 000. Physically, this three-particle-like interaction is the consequence of the presence of an internal vibrational mode of a particular type in the system. For a possible explanation, let us recall that if the model is integrable, such as the sG model, the solitons' motion may slow down before the collision but they can overcome the repulsive barrier and pass through each other. Here, the system is not integrable; the motion of the two kinks slows down more because a part of their kinetic energy is transferred to the internal mode. As a result they cannot pass through each other and stay at some minimum distance. The oscillation of their position is likely to be due to the complex interactions of the two solitons which are in an excited state. This example suggests that the internal mode of the solitons can play an important role in their dynamics.

3.3.2. Head-on collision between a 2π-kink and a 2π-antikink. The results obtained from the numerical computation of single-soliton dynamics and that of the collision processes of the soliton with the same topological charge, described above, have given a valuable qualitative description. However, for a quantitative description, we still need to simulate kink–antikink head-on collision at different ranges of magnetic field and deformability parameters, for allowed ranges of the initial velocities, through the discrete equations of motion (2.18*a*) and (2.18*b*). The lattice size is still $N = 200$ and we work here with the same conditions of parameters and numerical scheme as in the case of the two-2π-kink collision. The only

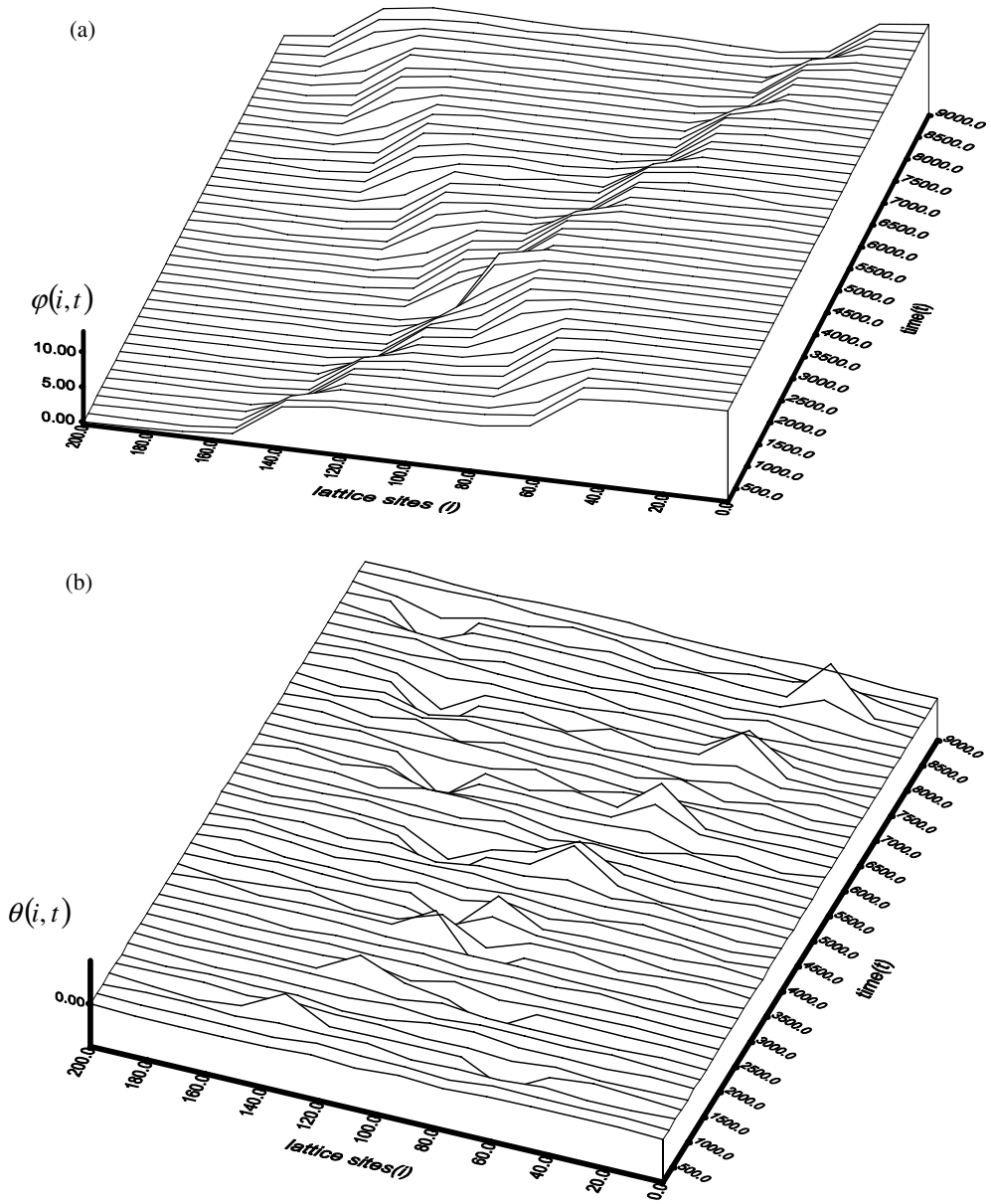

Figure 6. Head-on collision for a 2π-kink and a -2π-kink (equivalent to a 2π-antikink and a 2π-antikink collision) for the spin motion of the in-plane component (a) and the derived pulse–pulse collision of the out-of-plane spin motion (b) for the reduced magnetic field of $b = 0.5$ and the deformability parameter of $r = 0.5$. (c) A three-particle interaction as a result of a head-on collision between a 2π-kink and a -2π-kink (equivalent to a 2π-antikink and a 2π-antikink collision) for the reduced magnetic field of $b = 0.21$, and the deformability parameter $r = 0.6$, with an initial velocity of $v = 0.52$.

difference comes from the opposite sign on the topological charge of the initial conditions. The initial positions of the two excitations are chosen with a distance of 100 spin–lattice sites in order to avoid any possible interference between them at the beginning of the process. Note that for all the simulations, the processes were more rapid for $r > 0$ than in the case of $r < 0$.

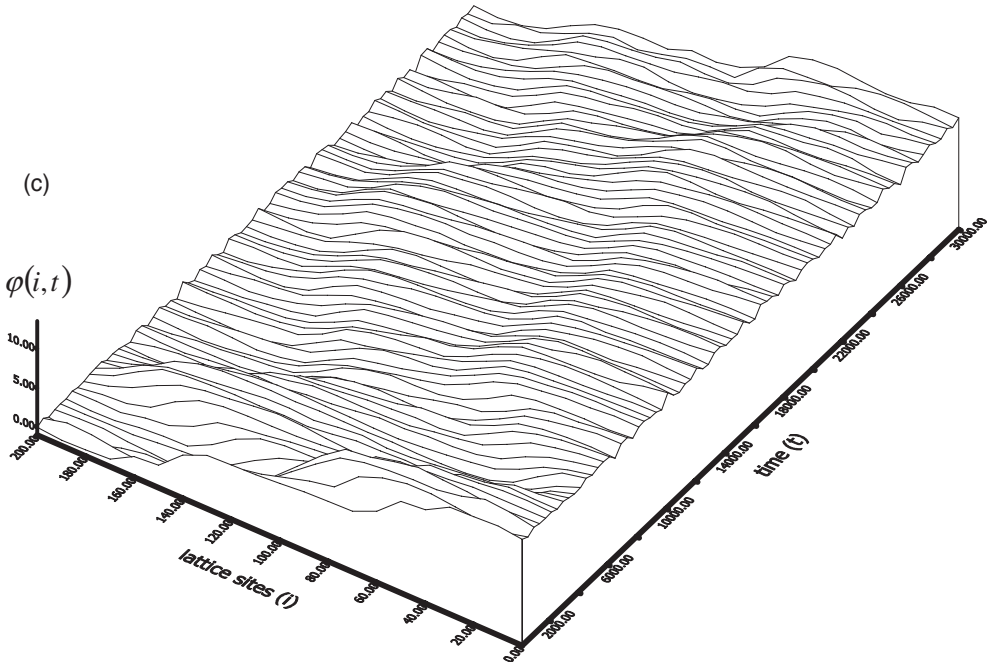

Figure 6. (Continued.)

This is in agreement with figure 2 where we plotted the velocities against the deformability parameter. So, in order to accelerate the process for a while, for negative values of r, it was necessary to choose a higher order of initial velocities of $v \geqslant 0.7$.

Let us first present figures 7(a) and (b) where we plotted the in-plane and the out-of-plane spin component collision processes, for $r = -0.3$ and $b = 0.45$ with initial velocity $v = 0.4$, respectively. These figures display a reflective phenomenon after any collision for the in-plane spin component, whereas the out-of-plane component is flipped (see figure 7(b)). Note that this phenomenon is also possible with a faster process for $r = 0.6$ and $0.3 \leqslant b \leqslant 0.65$ with $v = 0.34$. We also observed a few radiations of small amplitude waves on the shapes of the out-of-plane component after each collision. This reflective phenomenon is a good indication of the fact that the soliton obtained in this range of parameters can propagate and survive for a long time whenever it interacts with another soliton. This is also an indication of the fact that the discrete system of equations (2.18) is at least nearly integrable. Figure 8(a) is a schema obtained for $r = -0.8$, $b = 0.1$, when the initial velocity is $v = 0.9$ that illustrates the creation of a radiationlessly standing bound state of a 2π-kink and a 2π-antikink after their collision; this phenomenon can happen for the initial velocities with range $0.84 \leqslant v \leqslant 0.93$. This can be understood by the fact that, as long as the kink and antikink are sufficiently far apart, there is no radiation visible. So in such a condition, radiation losses are negligible. For the same parameters, figure 8(b) also illustrates at exactly what time each of the excitations stops moving and remains static as long as the process is produced. This is a good indication of a non-elastic but attractive interaction of the two excitations in the deformable spin chain. Since there is no internal oscillation observed, we have deduced that this is a zero-frequency translational mode formation. It is needless to mention the fact that, for the same value of the deformability parameter i.e. $r = -0.8$ and the reduced magnetic field, there is a window for the reduced velocities in the range $0.94 \leqslant v \leqslant 0.99$ where the collision process of the two

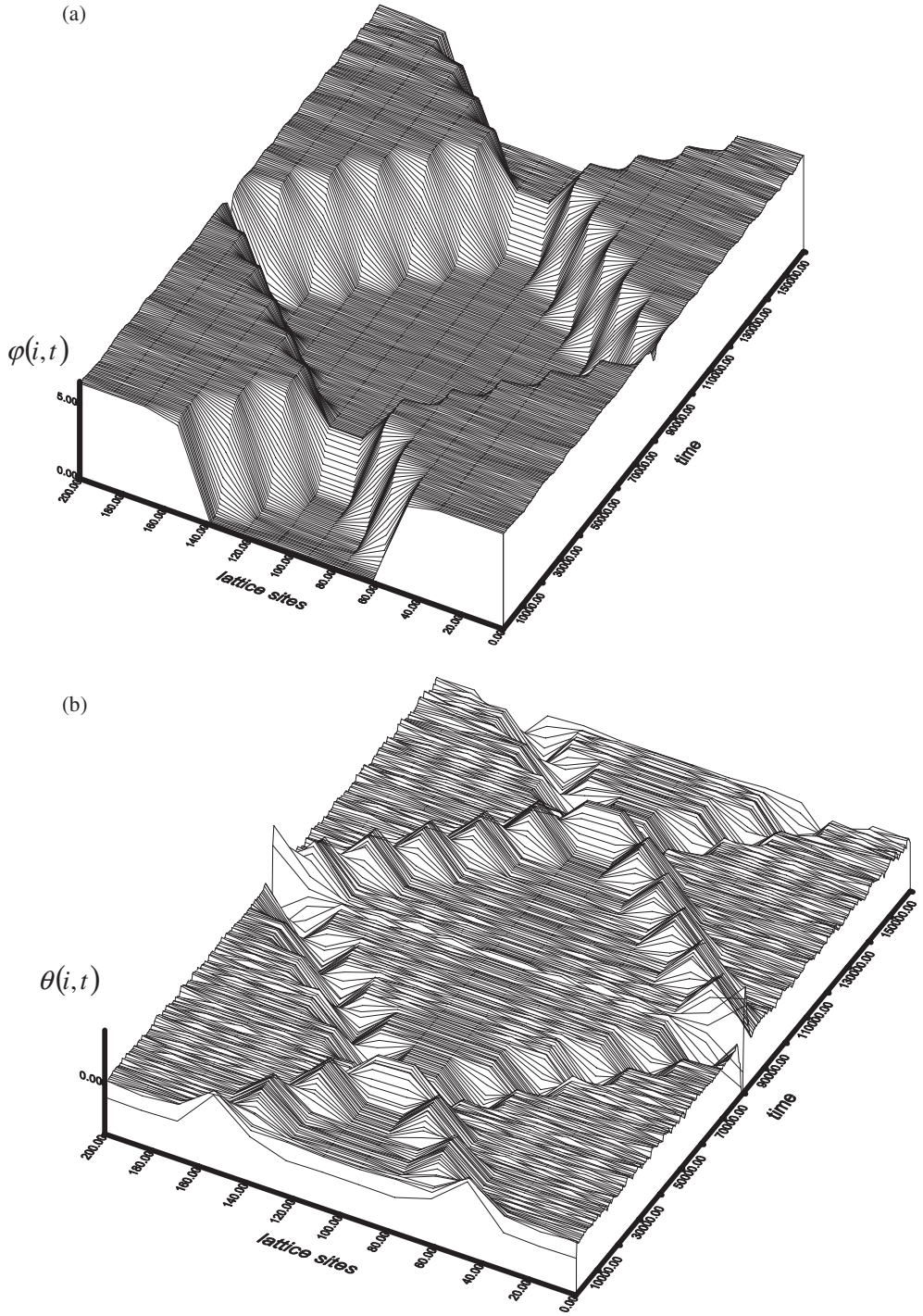

Figure 7. Head-on collision for a 2π-kink and a -2π-antikink for the spin motion for the parameters $r = -0.3$ and $b = 0.45$ with the initial velocity of $v = 0.4$: (a) in-plane component motion, where we observe an elastic collision that is produced as a reflective process for each of the two excitations; (b) out-of-plane component motion, where we observe an elastic collision that is produced as a reflective process for each of the two excitations but with a reversion of the orientation of their amplitude after each collision.

excitations results first in a breather formation that finally disintegrates in the chain. Thus, these velocity windows for a collision process lead to an annihilation phenomenon. This strong pinning of the two kinks is also displayed in the dynamics of the one-component deformable soliton model [38, 39]. For the parameters $r = 0.9$, $b = 0.5$ and $v = 0.65$, we observe in figures 9(a) and (b) that, with periodic boundary conditions, the first collision happens at the chain's end. After this first collision, the in-plane spin component comes out with a new shape, which is constituted of a new kink shape with a reduced size very close to that of a π-kink. Then, the resulting solitons continue the collision process both at the middle and at the chain's end with some slight radiations. But these radiations do not alter the collision processes because, after any collision, these solitons with new shapes display a very robust behaviour. The out-of-plane component also displays a robust behaviour through the collision process with a scenario of mutual crossing without flipped shape while keeping the same size. Therefore, this is a good indication that with these parameters soliton solutions exist for the discrete system of equation (2.18), whenever their shape may differ from those of the initial conditions. From figures 10(a) and (b), we do observe a scenario of four-particle interactions as a result of a collision process engaged between the two excitations of the different spin components. It is clear from these figures that, when the in-plane excitations are introduced in the chain, some time later, while moving towards each other, each of them is divided into two excitations moving in opposite directions. Therefore, the collision scenario becomes that of a kink and an antikink that are the first to collide at the middle of the chain. At the same time, the two other excitations engaged in the collision process display opposite directions while moving and this would lead to their collision at the end of the chain. The same collision scenario occurs for the initial two excitations engaged for the out-of-plane component. The difference here comes from the fact that within the four-particle interactions, the first couple of excitations that first faced the collision displays a reversed pulse shape while the second couple of excitations displays the ordinary pulse shape. We also notice for the two spin components that the first couple of excitations that first faced the collision at the middle of the chain does collide with the other excitations of the second couple before the second couple finally faces its first collision. Hence, the first couple's motion is faster than that of the second couple.

4. Summary and concluding remarks

Since the previous studies on the numerical simulations of the soliton dynamics in a rigid Heisenberg chain [5, 48] were fairly complete and that of a deformable magnetic chain [35] involved a tremendous amount of numerical calculation, it is not our aim here to perform similar studies on the deformable spin model. For instance, Etrich *et al* [48] have shown that in the discrete ferromagnetic spin chain two essentially different static in-plane soliton structures may occur: one with its centre located on a lattice site, the so-called central-spin configuration, and the other with its centre located in the middle between two neighbouring spin–lattice sites, which is the so-called central-bon configuration. This kind of specification arises from a deep study of the discreteness effects on the soliton dynamics. We will address these problems in a future publication. Here, we only wanted to stress a few points that bring new features to the soliton dynamics in a ferromagnetic chain when the deformability effects are considered.

Finally, to summarize, we have been able to examine the limit of the validity of the implicit soliton solution by a numerical computation in a classical deformable easy-plane ferromagnetic chain of the Heisenberg model, for the deformability parameter in the range of $-1 < r < 1$. Modifying the Zeeman energy of a Heisenberg chain, we have analysed the nonlinear dynamics of the soliton structures taking the model of $CsNiF_3$ material as a

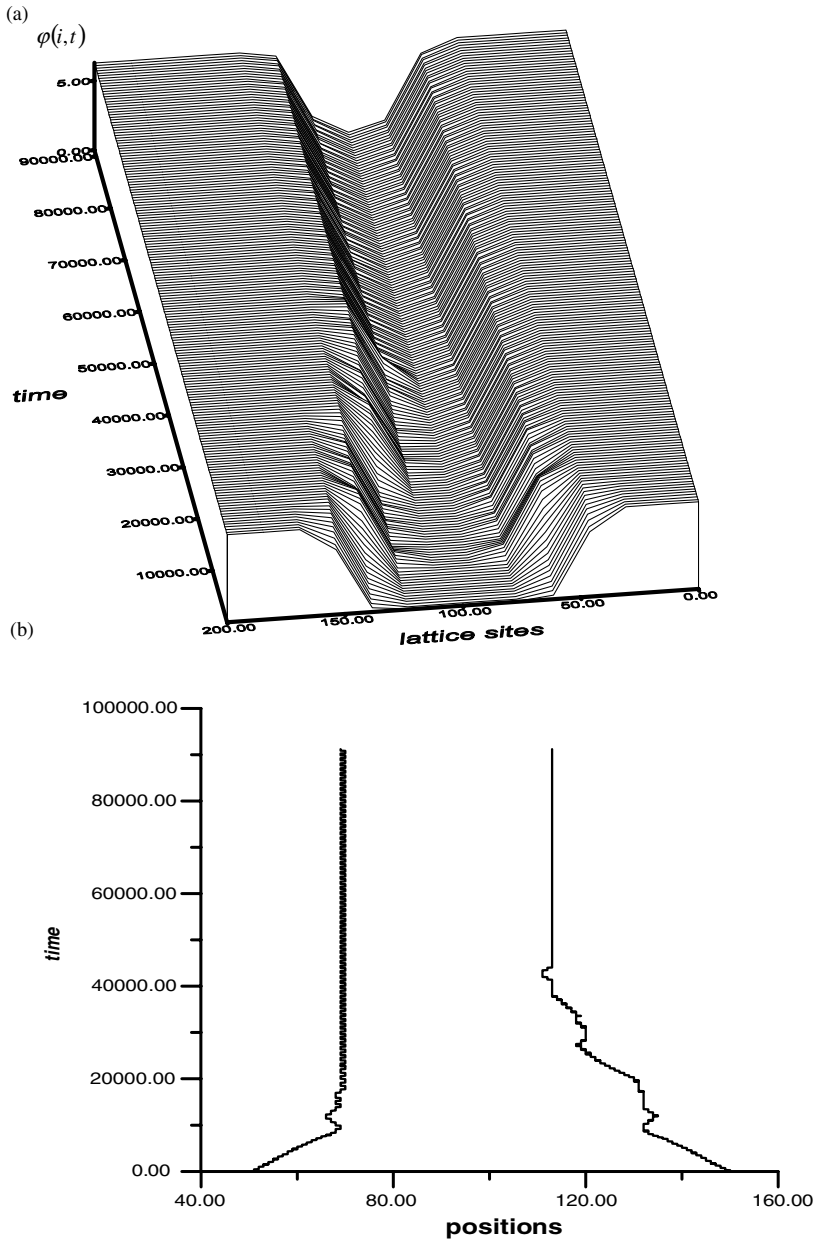

Figure 8. (a) Creation of a standing bound state of a 2π-kink and a 2π-antikink after their collision for deformability parameter $r = -0.8$ and the reduced magnetic field $b = 0.1$ with initial velocity $v = 0.9$. (b) Contour plot of the positions against time of the two excitations engaged in the collision process. This schematic diagram illustrates at exactly what time each of the excitations stops moving and remains static as long the process is produced.

particular example. The different simulations of the single soliton's propagation point out that, for some particular values of the deformability parameters, the motion of the kink (in-plane component) on a double periodic oscillating background can happen for any subsonic velocity in a discrete ferromagnetic chain under deformability effects. From a physical point

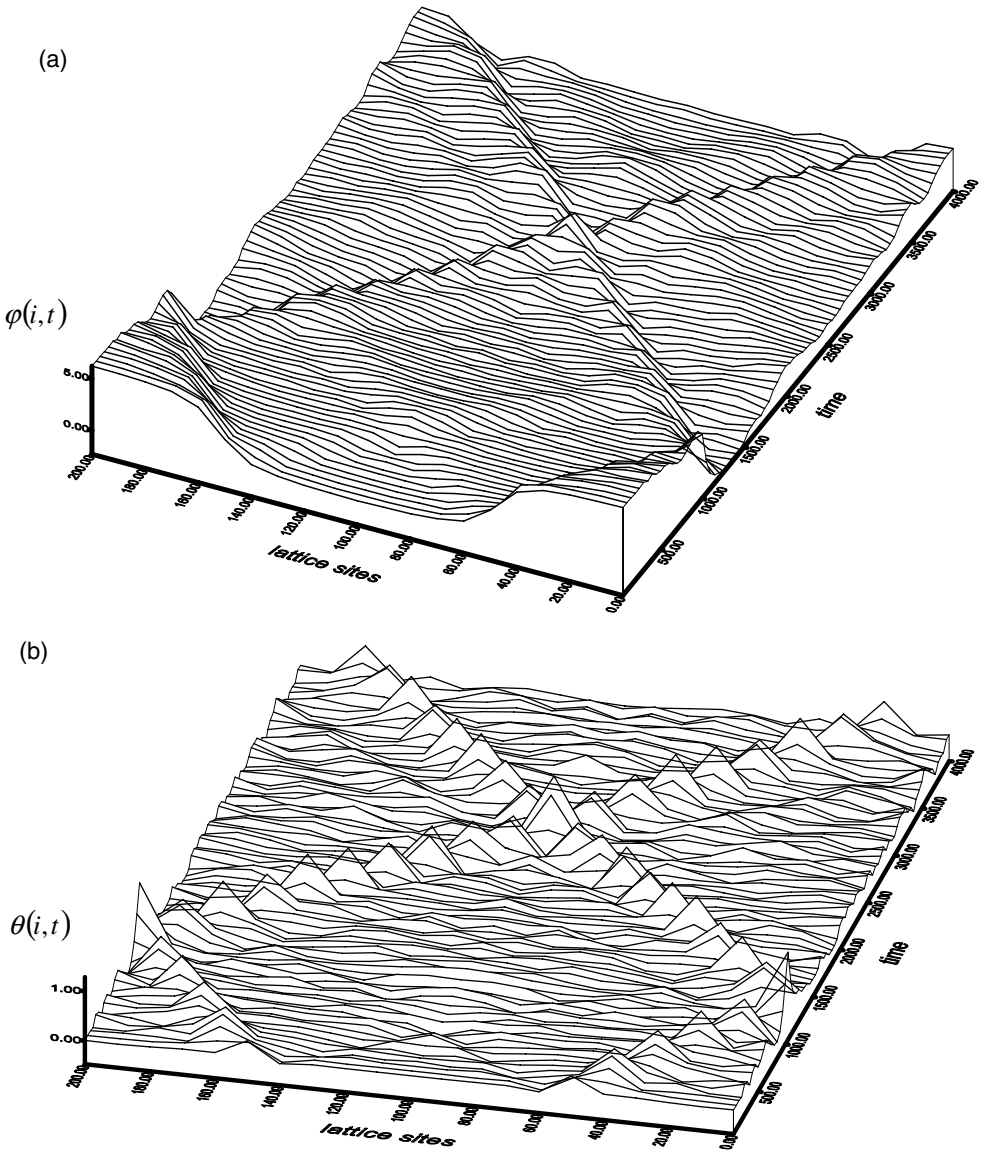

Figure 9. (a) Creation of new kink and antikink solitons with reduced shape after the first collision of the initial conditions for deformability parameter $r = 0.9$ and the reduced magnetic field $b = 0.5$ with initial velocity $v = 0.6$. (b) Mutual crossing of the out-of-plane spin component during the colliding processes of the two excitations with size conserved and no flipping shape.

of view, this kind of motion that is conducted by the nanopteron wave type is the result of a nonlinear interaction of a kink with a wave propagating along the chain. From this interaction, it happens that a bound state of a kink and the wave is created in such a way that the wave pushes the kink, on the one hand, and the wave is finally pinned to the kink, on the other hand. Therefore, some kind of dynamical self-trapping of a kink and the wave takes place. This mechanism finally reduced the bound state velocity to that of a subsonic wave. It has also been possible to find a non-oscillating kink for the in-plane spin component angle and the corresponding pulse for the out-of-plane spin component angle as a solution of the nonlinear

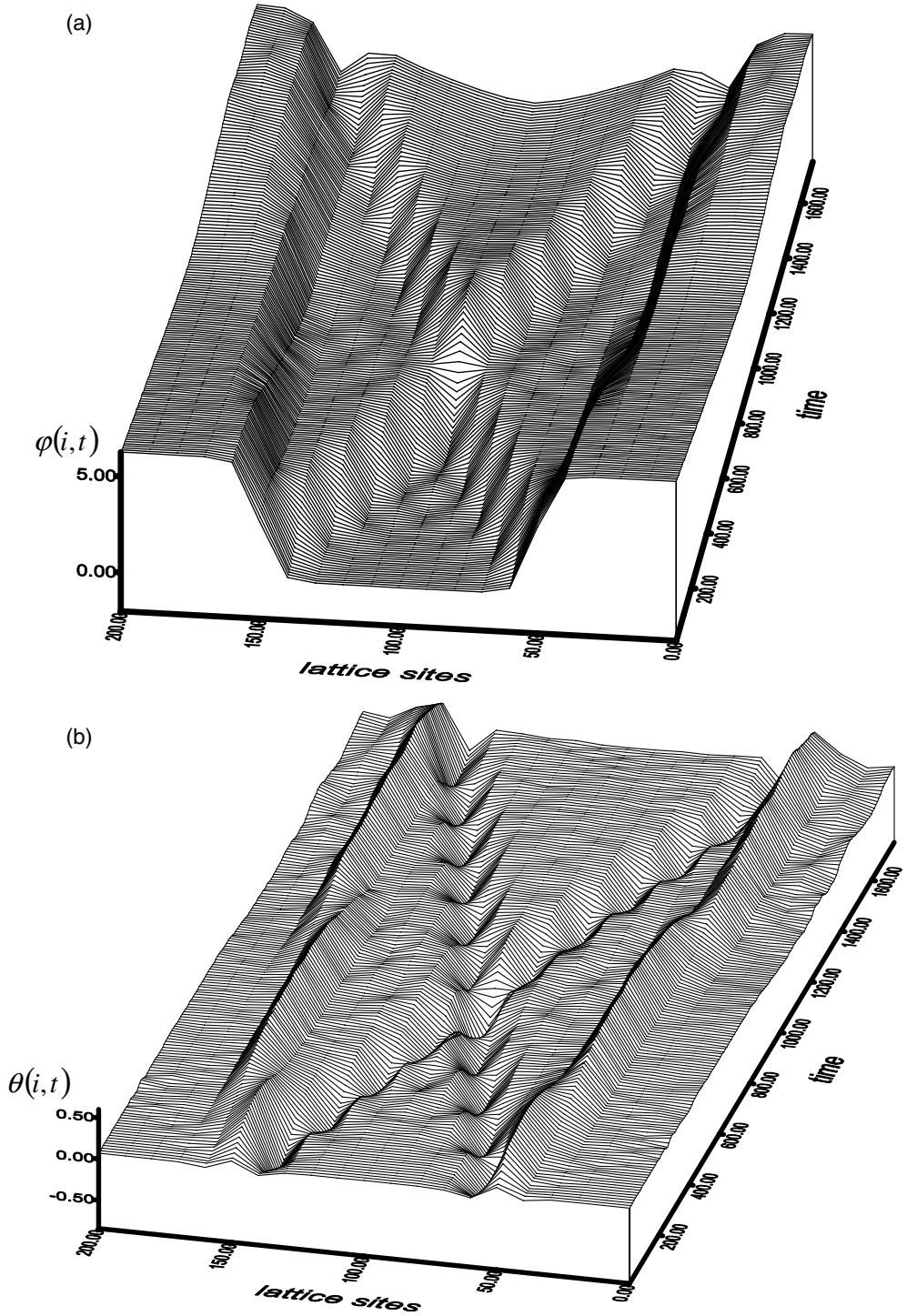

Figure 10. Collision process for the in-plane and the out-of-plane components for the parameters $r = 0.8$, $b = 0.02$ and initial velocity $v = 0.52$. (a) From the two initial excitations we came out with a four-particle interaction constituted of two couples of a kink and an antikink. (b) From the two initial excitations we came out with a four-particle interaction constituted of two couples of pulses with flipped shapes.

discrete coupled equations of motion for the magnetic chain. This is possible only for some finite number of preferred velocities and suitably chosen deformability parameters. A similar result for a moving kink concerning the discrete spectrum of the velocity has been obtained in [49] for a modified ϕ^4 model where one explicit kink solution is known. We also noticed from the kink–kink interaction that it was possible to find a moving or standing bound state of the same topological charge $Q = \pm 1$ to form a soliton of higher topological charge. These moving bound states display a free propagation behaviour and this was first discovered by Peyrard and Kruskal [31]. They interpreted this as a resonance interaction. We have also realized that the presence of an internal mode may result in a three-particle-like interaction that manifests itself with an alternation between an attractive and a repulsive interaction that happens between the two excitations of kink type engaged in the collision while keeping a minimum distance between them. Within this minimum distance is located a nonlinear wave whose length varies from a minimum to the maximal values. Moreover, from kink and antikink interaction simulations, we have obtained on the one hand a standing bound state of a kink and antikink, and on the other hand a four-particle interaction. This four-particle interaction is obtained as result of the creation of a second pair of a kink and an antikink of reduced size (for the in-plane component) and a second pair of pulses moving towards each other for the out-of-plane component. The final collision scenario is that of four excitations of soliton type interacting in the magnetic chain for both of the spin components. Most of the bound states described above show that the dynamics of the two-component magnetic system preserves the properties of the one-component deformable soliton model [39, 41]. Hence, the other new processes described above are features of deformability effects on discrete deformable ferromagnets. Thus, the existing results demonstrate the importance and the potential of a simple, intuitive and physically appealing picture, which, even if it might not be quantitatively correct, reasonably describes the complex dynamics and certainly stimulates further experiments on magnetic model systems. The fundamental question for the existence of the implicit soliton in a one-dimensional magnet, as suggested by our theory, appears to have been answered positively by our numerical experiments. Further computational, experimental and theoretical efforts should now aim at the investigation of details of these implicit soliton-like bearing systems. This in particular calls for more theoretical work to establish an analytical expression of the critical magnetic field (which is actually very difficult to derive) for these implicit solitons and compare it to its corresponding numerical value. We also expect that an important role of this modified Zeeman energy in our magnetic model for future investigations, both theoretical and experimental, will be to clarify the transition between the ballistic, the stochastic and the diffusive behaviour for the dynamics [35], and investigate a possible induction of phase transition for the thermodynamics in a 1D Heisenberg model.

In order to give indication of possible experiments, we should recall that harmonic generation has become more and more important in efficiently generating new frequencies for various applications. In this way, Bhattacharya *et al* [50] have reported results of an experiment that uses the generation of harmonics of a low frequency and small amplitude modulation signal to probe the nature of nonlinearity associated with the standard current–voltage measurement and determines the form of the current carried by the charge-density-wave conductor $NbSe_3$ near the threshold. The harmonic-generation experiment was performed by adding a small (6 μA) ac current source from a Hewlett-Packard model HP3562 A dynamic signal analyser at typically 100 Hz. The critical exponent obtained in this experiment is consistent with a cooperative dynamical critical phenomenon involving many degrees of freedom of a deformable charge-density wave [51, 52]. Also, Gullikson and Mills [53] reported measurements of the positronium work function as a function of temperature and used it to derive the positron deformation potential for Al. The experiments were performed

using a magnetically guided beam of slow positrons in an ultrahigh vacuum chamber with a base pressure of 2×10^{-10} Torr. In addition, in the context of nonlinear crystals, backward second-harmonic generation (SHG) has been observed using subpicosecond and nanosecond laser pulses in periodically poled lithium niobate crystals [54]. Furthermore, backward third-harmonic generation (THG) based on cascaded second-order nonlinear processes [55] has been also observed. In this THG, the first crystal is used for sum-frequency generation. Since the cascaded second-order nonlinear process was demonstrated [56], higher order harmonics [57] have also been observed via cascading. It should be noted that the harmonic generation coincided with the significantly improved high quality nonlinear optical materials such as KH_2PO_4 (KDP) and $KTiOPO_4$ (KTP), as well as discoveries of new materials such as β-BaB_2O_4 (BBO) and LiB_3O_3 (LBO). Concerning soliton theories in magnetic systems, most of the experimental apparatus in these studies have been described previously [5]. $CsNiF_3$ is the prototype of a quasi-one-dimensional ferromagnetic compound and has been investigated in detail using many different experimental methods, such as susceptibility measurements [58–61], neutron diffraction [62, 63], specific heat measurements [59] and inelastic neutron scattering [64, 65]. However, while for rigid magnetic systems the different proposed models have easily found experimental verifications, in the deformable case there are not yet experimental counterparts to the few theoretical proposals [34, 38, 39, 41]. These experimental investigations of deformable solitons have been hampered by the apparent need for nanomagnets and experimental apparatus to produce deformability. For example, time-dependent modulation of the bias energy can be achieved by an ac electric field coupled to the dipole moment of the two-state system, or in a superconducting quantum interference device (SQUID) ring device, by a time-dependent external field threading the ring. In contrast, 'quadripole'-like couplings induce a variation of barrier height and width and thus lead to a modulation of the tunnelling matrix element (TME). Promising candidates to study the effects of concerned harmonic modulation of the bias and TME are the variable barrier rf SQUID ring [66, 67] and magnetic molecular clusters in longitudinal and transverse ac magnetic fields [68] such as Mn_{12} [69] and Fe_8 [70] nanomagnets. However, the deformable effect is a more complicated physical phenomenon and appears to constitute an interesting laboratory for the examination of deformable models via parametric process (quasi-phase matching) and parametric modulational instability. Again the experimental activity also seems to be growing on account of the existence of out-of-plane instabilities as well as a soliton spectrum quite different from the sG results.

Acknowledgments

Dr Nguenang Jean-Pierre would like to thank the International Centre for Theoretical Physics (AS-ICTP) and the Swedish International Development Agency (SIDA) for sponsoring his Visit as a Junior Associate at the AS-ICTP.

We would like to acknowledge helpful suggestions and a critical reading of our manuscript by Professor Alexander A Nersesyan of the condensed matter group of the Abdus Salam ICTP. We also acknowledge helpful suggestions of Professor Michel Peyrard of Laboratoire de Physique of Ecole Normale Supérieure de Lyon in the final version of this paper.

References

[1] Bishop A R and Schneider T (ed) 1978 *A General Review in Solitons and Condensed Matter Physics* (New York: Springer)

Bishop A R, Pokrovsky V L and Tognetti V (ed) 1991 *Microscopic Aspect of Nonlinearity in Condensed Matter* (New York: Plenum)

Bishop A R, Ecke R and Gubernatis J (ed) 1992 *Nonlinearity in Material Science* (Amsterdam: North-Holland)

[2] Frenkel J and Kontorova T 1939 *J. Phys. (Moscow)* **1** 137
[3] Seeger A and Schiller P 1966 *Physical Acoustics* vol 3A, ed W P Mason (New York: Academic)
[4] Flytzanis N, Crowley S and Celli V 1977 *Phys. Rev. Lett.* **39** 891
[5] Mikeska H J and Steiner M 1991 *Adv. Phys.* **40** 191
[6] Krumhansl J A and Schriffer J R 1975 *Phys. Rev.* B **11** 3535
[7] Prelovtsek P and Sega I 1981 *J. Phys. C: Solid State Phys.* **14** 5609
Ishibashi Y 1979 *J. Phys. Soc. Japan* **46** 1254
[8] Ngabireng C M and Kofane T C 1997 *Phys. Scr.* **55** 257
[9] Boucher J P, Regnault L P, Rossat-Mignot J, Renard J P, Bouillot J and Stirling W G 1980 *Solid State Commun.* **33** 171
[10] Nguenang J P and Kofané T C 1997 *Phys. Scr.* **55** 367
[11] Rice M J, Bishop A R, Krumhansl J A and Trullinger S E 1976 *Phys. Rev. Lett.* **36** 432
[12] Axel F and Aubry S 1981 *J. Phys. C: Solid State Phys.* **14** 5433
[13] Bruce D A 1980 *J. Phys. C: Solid State Phys.* **11** 4615
[14] Su W P, Schriffer J R and Heeger A J 1979 *Phys. Rev. Lett.* **42** 1698
Su W P, Schriffer J R and Heeger A J 1980 *Phys. Rev.* B **22** 2099
[15] Grundberg P, Schreiber R, Pang Y, Brodsky M B and Sowers H 1986 *Phys. Rev. Lett.* **57** 2442
[16] Baibich M N, Broto J M, Fert A, Nguyen van Dau F, Petroff F, Etienne P, Creuzet G, Friederich A and Chazelas J 1988 *Phys. Rev. Lett.* **61** 2472
[17] Wang R W, Mills D L, Fullerton E E, Mattson J E and Bader S D 1994 *Phys. Rev. Lett.* **72** 920
[18] Micheletti C, Griffiths R B and Yeomans J M 1997 *J. Phys. A: Math. Gen.* **30** L233
[19] Coppersmith S N and Littlewood P B 1987 *Phys. Rev.* B **36** 311
[20] Mikeska H J 1980 *J. Phys. C: Solid State Phys.* **13** 2913
Mikeska H J 1978 *J. Phys. C: Solid State Phys.* **11** L29
[21] Wysin G, Bishop A R and Kumar P 1984 *J. Phys. C: Solid State Phys.* **17** 5975
[22] Nguenang J P, Kofané T C, Yomba E and Yo J D 1999 *Phys. Scr.* **60** 460
[23] Nguenang J P and Kofané T C 2000 *Physica* D **147** 311
[24] Nguenang J P, Kenfack A J and Kofané T C 2002 *Phys. Rev.* E **66** 56613
[25] Magyari E and Thomas H 1982 *Phys. Rev.* B **25** 531
[26] Kumar P 1982 *Phys. Rev.* B **25** 483
Kumar P 1982 *Physica* D **5** 359
[27] Osano K 1984 *J. Phys. C: Solid State Phys.* **17** 843
[28] Magyari E, Thomas H and Weber R 1984 *Z. Phys.* B **55** 189
Magyari E, Thomas H and Weber R 1985 *Z. Phys.* B **62** 97
[29] Maki K and Takayama H 1980 *Phys. Rev.* B **20** 3223
Maki K and Takayama H 1980 *Phys. Rev.* B **20** 5002
[30] Curie Y F, Trullinger S E, Bishop A R and Krumhansl J A 1977 *Phys. Rev.* B **15** 5567
[31] Peyrard M and Kruskal M D 1984 *Physica* D **14** 88
[32] De Lacheisserie E 1993 *Magnetostriction: Theory and Applications* (Boca Raton, FL: CRC Press)
[33] Béranger G, Duffault F, Morlet J and Tiers J-F 1996 Cent ans après la découverte de l'Invar... les alliages de fer et de nickel *Technique et Documentation* Paris
[34] Kofané T C 1999 *J. Phys.: Condens. Matter* **11** 2481
[35] Nguenang J P, Kenfack A J and Kofané T C 2003 *Phys. Rev.* B submitted
[36] Hoogerbeets R, Wiiegers S A J, Van Duyneveldt A J, Willet R D and Geisen U 1984 *Physica* B **125** 135
[37] Magyari E and Thomas H 1992 *Phys. Scr.* **44** 45
[38] Remoissenet M and Peyrard M 1981 *J. Phys. C: Solid State Phys.* **14** L481
[39] Peyrard M and Remoissenet M 1982 *Phys. Rev.* B **26** 2886
[40] Tsukamoto A, Fijita T, Nakagawa K and Itoh A 1999 *Trans. Magn.* **35** 2998
[41] Savin A V, Zolotaryuk Y and Eilbeck J C 2000 *Physica* D **138** 267
[42] Bishop A R, Krumhansl J A and Trulinger S E 1980 Soliton in condensed matter: a paradigm *Physica* D **1** 1
[43] Jackiw R 1977 Quantum meaning of classical field theory *Rev. Mod. Phys.* **49** 681
[44] Willis C, El-Batanouny M and Stancinoff P 1986 *Phys. Rev.* B **33** 1904
[45] Stancinoff P, Willis C, El-Batanouny M and Burdick S 1986 *Phys. Rev.* B **33** 1912
[46] Peyrard M, Pnevmatikos S and Flytzanis N 1986 *Physica* D **19** 286
[47] Boyd J P 1990 *Nonlinearity* **3** 177
[48] Etrich C, Mikeska H J, Magyari E, Thomas H and Weber R 1985 *Z. Phys.* B **62** 97
[49] Flach S, Zolotaryuk Y and Klado K 1999 *Phys. Rev.* E **59** 6105
[50] Battacharya S, Higgins M J and Stokes J P 1989 *Phys. Rev. Lett.* **63** 1503

[51] Ficher D S 1983 *Phys. Rev. Lett.* **50** 1486
[52] Ficher D S 1985 *Phys. Rev.* B **31** 1396
[53] Gullikson E M and Mills A P Jr 1987 *Phys. Rev.* B **35** R8759
[54] Arbore M A, Fejer M M, Fermann M E, Hariharan A, Galvanauskas A and Harter D 1997 *Opt. Lett.* **22** 13
[55] Ding Y J, Kang J U and Khurgin J B 1998 *IEEE J. Quantum Electron.* **34** 967
[56] Yablonovitch E, Flytzanis C and Bloemberger N 1972 *Phys. Rev. Lett.* **29** 865
[57] Sundheimer M L, Villeneuve A, Stegeman G I and Bierlein J D 1994 *Electron. Lett.* **30** 975
[58] Steiner M, Krueger W and Babel D 1971 *Solid State Commun.* **9** 227
[59] Levesque J V, Snel J and Smith J J 1973 *Solid State Commun.* **13** 371
[60] Dupas C and Renard J P 1975 *Proc. 14th Int. Conf. on Low Temperature Physics* vol 55 (Amsterdam: North-Holland)
Dupas C and Renard J P 1976 *Solid State Commun.* **20** 581
Dupas C and Renard J P 1977 *J. Phys. C: Solid State Phys.* **10** 5057
[61] Lebesque J V and Huyboom N F 1976 *Comment. Phys.* **1** 33
[62] Steiner M 1972 *Solid State Commun.* **11** 73
Steiner M 1979 *J. Appl. Phys.* **50** 7395
Steiner M 1979 *Solid State Commun.* **67** 5593
[63] Steiner M and Dachs H 1974 *Solid State Commun.* **14** 841
[64] Steiner M and Dorner B 1973 *Solid State Commun.* **12** 537
[65] Steiner M, Dorner B and Villain J 1975 *J. Phys. C: Solid State Phys.* **8** 165
[66] Han S, Lapointe J and Lukens J E 1991 *Phys. Rev. Lett.* **66** 810
[67] Han S, Lapointe J and Lukens J E 1992 *Phys. Rev.* B **46** 6338
[68] Wernsdorfer W and Sessoli R 1999 *Science* **284** 133
[69] Friedman J R *et al* 1996 *Phys. Rev. Lett.* **76** 3830
[70] Sangregorio C *et al* 1997 *Phys. Rev. Lett.* **78** 4645